1

Study on Method for Relative Fidelity Preservation of Seismic Data

1.1 Introduction

The reservoir of lithology formation, under the control of multiple factors such as regional structures and depositional facies belt, shows some distribution regularity and also has significant exploration potential. However, the exploration challenge is relatively great due to their complex concealment. In recent years, China has made great breakthroughs and discoveries in this field, proving favorable and huge remaining resource potential; this has gradually become the major field of reservoir gain in China [1–4].

The lithology analysis of these lithology reservoirs poses high requirements for the seismic data processing [5–7]. The first challenge is to increase the resolution of seismic data, so as to identify the geologic features like thin sand layers and sand body pinch-out points, on the processed seismic data. Second, to preserve the amplitude, and not damage the module of amplitude relation between adjacent seismic traces on processing flow. However, previous study mainly focused on identifying thin layers, increasingly widening the frequency band of seismic data and improving the dominant frequency. Therefore, a lot of high-resolution seismic processes have been developed for the purpose of increasing seismic dominant frequency.

Increasing the resolution of seismic data is mostly realized by deconvolution method [8–19], which is an important means in seismic data processing. In order to increase the resolution of seismic data, an operator for high frequency deconvolution is devised to identify thin layers. However, which principles should be used to determine the frequency bandwidth and dominant frequency of operator for high frequency deconvolution? Is it possible to increase the dominant frequency of the operator for high frequency deconvolution without restriction? These are the questions that remain to be discussed.

Figure 1.1 presents the comparison of lithology reservoir seismic profiles through SN31 wellblock in the Luxi area of Junggar Basin. In Figure 1.1a, a high-resolution and high-S/N seismic processing technology was adopted. The lithology reservoir of J2t0 of SN31 wellblock was interpreted from the seismic profile shown in the figure (it also proved to be sand reservoir through drilling), but from the profile, the continuity of J2t0 reservoir was favorable (in the location of Well S302, the J2t0 extended for more than 1 km to the updip direction of the
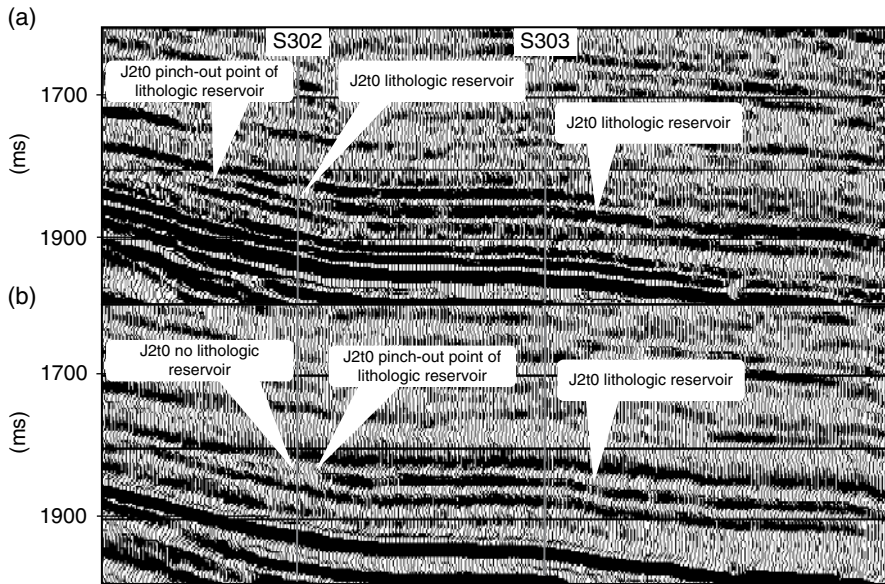
(a)

(b)

Figure 1.1 Comparison between (a) conventional seismic profile and (b) relative fidelity seismic profile through wells S302 and S303.

reservoir until the lithology reservoir pinched out). For this purpose, a number of wells were planned for this complete lithology reservoir. Wells S302 and S302 shown on the figure were among them, but their drilling effectiveness varied greatly. The reservoir in Well S303 is very good and the well is a high oil producer, while reservoir in Well S302 is poor (lithology varied, and J2t0 reservoir is mainly mudstone).

From the analysis of the data on Figure 1.1, it was believed that the over emphasizing on the high resolution and high SNR during processing deteriorated the fidelity of processed results, directly resulting in the distortion of lithology reservoir seismic response that was reflected on seismic profile.

On seismic profile, the display reliability of seismic response on lithology reservoirs is subject to the fidelity of seismic processing. Currently, it is very difficult to realize absolute seismic fidelity preservation processing, but relative fidelity preservation processing is possible. Figure 1.1b shows the relative fidelity preservation profile that was reprocessed as per the flowchart in Figure 1.13, in 2006. As clearly shown in the figure, the reflection of J2t0 reservoir in Well S302 is very weak, indicating that the reservoir is no longer present. The pinch-out point of J2t0 reservoir identified on seismic profile is nearly 300 m to downdip direction of lithology reservoir in Well S302, which matches with the data of Well S302 that has been completed.

This has raised a question: the processing of seismic data is the key in exploration of lithology reservoirs. Only when the seismic response of reservoir properties is truly reflected on the profile after seismic processing to the greatest extent can the seismic data be effectively used to identify the lithology reservoirs.

In view of the above problems, we made analysis by selecting a 2D high-resolution pilot line of 8 km from the Shidong area in the Junggar Basin across Wells Shidong-2 and Shidong-4, on the results of high resolution and high SNR processing and relative fidelity preservation processing. Based on this, we came up with a processing method for relative fidelity of seismic data.

Relative fidelity preservation processing[5] of seismic data should pay attention to the following items: (1) Protection of effective frequency band. The widening of effective band should rely on SNR of seismic data. In order to widen the low S/N seismic data to high frequency band, it is necessary to control the bandwidth and dominant frequency of the deconvolution operator. The main function of deconvolution is to increase the energy of high frequency components within the effective band so as to prevent notch frequency at effective high frequency band. (2) Protection of low frequency, especially that of 3–8 Hz. The scenarios that suppress low frequency data of 10 Hz and below in high resolution and high SNR processing, or give significant loss of effective low frequency information with adoption of strong f-k noise elimination should be avoided. (3) Amplitude preservation. Modification modules like RNA should not be applied to avoid damaging the lateral relationship of seismic channel amplitude. (4) Phase preservation. The module should not be used as it may damage the phase position in processing, while the zero phase deconvolution and surface consistent deconvolution will not damage the phase relation. Compared with the profile processed by high resolution and high SNR, the profile processed by relative fidelity preservation could reflect the seismic effect on subsurface sand reservoirs quite genuinely.

While discussing the processing method of relative fidelity preservation processing or high-resolution and high SNR processing, the effect of seismic acquisition manner on seismic data processing is also elaborated in this book. Seismic broadband acquisition is the basis for relative fidelity preservation processing. Based on the seismic pilot survey line, we analyzed and discussed the effects of seismic acquisition source and observation means on the data processed by high resolution and high SNR or by relative fidelity in terms of profile reflection features and spectrum features.

1.2 Discussion on Impact on Processing of High-resolution, High SNR for Seismic Acquisition and Observation Mode

Figure 1.2 is the t_0 contour of the sand bottom boundary in the Cretaceous Qinshuihe Formation of the Shidong area in the Junggar Basin. It is located in the distribution area of the oil layer of the Qingshuihe formation in Well Shidong No. 2 region and Well Shidong No. 4 region, which is highlighted by yellow in the figure. But based on the previous seismic data, it is really difficult to explain the reservoir distribution characteristics of these two wells. Therefore, in 2002, seismic pilot survey lines (blue line) across Wells Shidong No. 2 and Shidong No. 2 were deployed to study and find out a method for
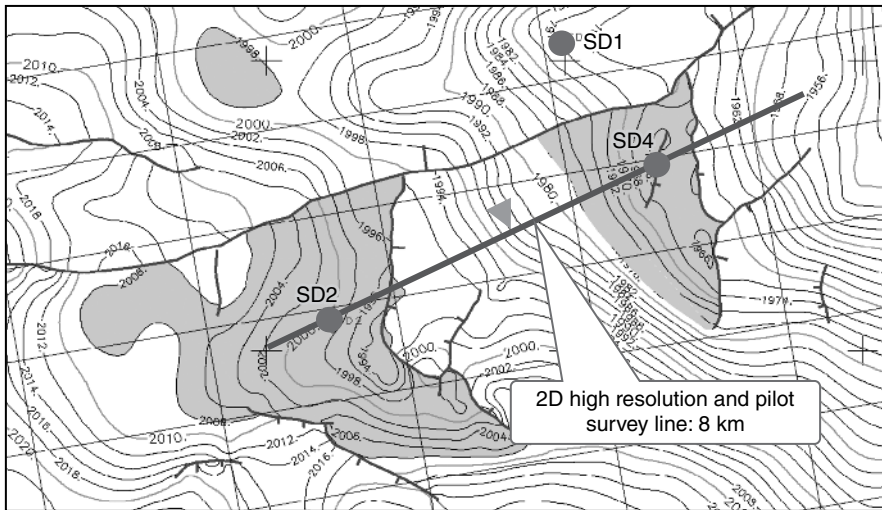
Figure 1.2 The t_0 contour of the sand bottom boundary in Cretaceous Qinshuihe Formation of Shidong area.

improving the quality of field seismic data acquisition, thus meeting the requirements of lithology reservoir exploration.

The seismic pilot survey lines across Well Shidong No. 2 and Shidong No. 4 is 8 km long, with acquisition factors including: (1) Single well excitation: excitation well depth is 85 ~ 139 m; the dosage of explosive per well is 4 kg and the number of wells is 1, so the total dosage for single well excitation is 4 kg. The offset distance is 50 m. The number of receiving channels is 1200 and the distance between channels is 5 m (or 240 receiving channels with a 25 m interval). (2) Combined well excitation: excitation well depth is 6 m; the dosage of explosive per well is 2 kg and the number of wells is 10, so the total explosive dosage is 20 kg. The offset distance is 50 m. The number of receiving channels is 1200 and the distance between channels is 5 m (or 240 receiving channels with a 25 m interval). (3) Controllable seismic source excitation: 4 seismic sources multiplied by 6 times and the scan frequency is 8 ~ 90 Hz. The offset distance is 25 m. The number of receiving channels is 300 and the distance between channels is 25 m. High resolution and high SNR process (Figure 1.2) were used to increase the resolution of seismic data and find out the reservoir distribution characteristics in the Qingshuihe formation between Well Shidong No. 2 region and Well Shidong No. 4 region. In data processing, zero phase deconvolution was used both at prestack and poststack in order to increase the resolution; additionally, the random noise attenuation modification was employed to improve the signal-to-noise ratio.

We analyzed the processing progress based on the five control points shown in Figure 1.3: original single shot record frequency scan (control point ①, Figure 1.4); upon the completion of the first arrival refraction static correction process, we used the single shot record and spectrum analysis results of target layer (control point ②, Figure 1.5) to analyze the quality of data. After completing prestack
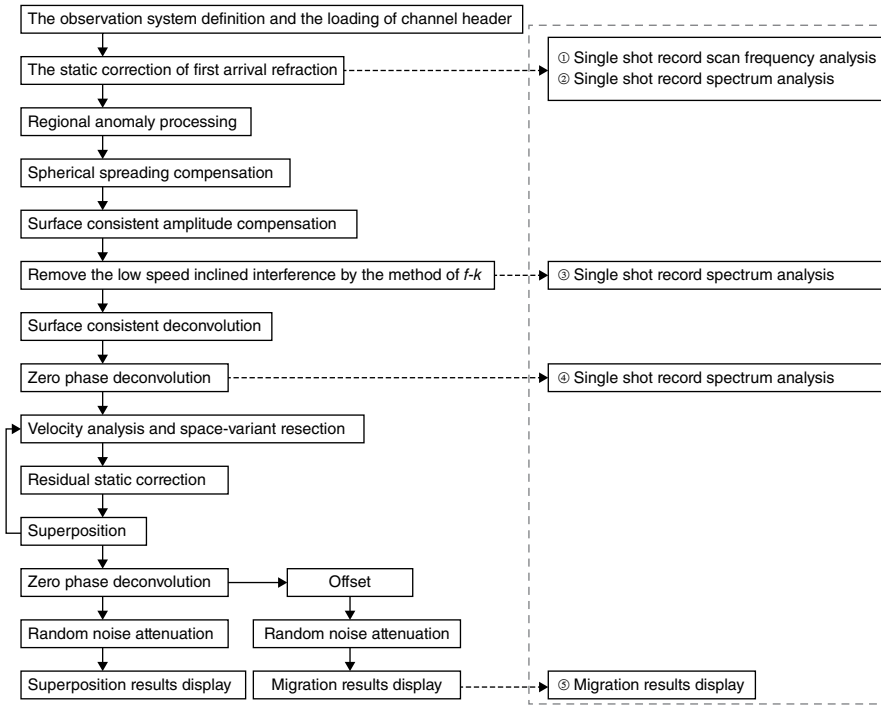
```
┌─────────────────────────────────────────────────────────┐
│ The observation system definition and the loading of channel header │
└─────────────────────────────────────────────────────────┘
                          │
                          ▼                          ┌─────────────────────────────────────┐
┌─────────────────────────────────────┐     ┌ ─ ─ ─│ ① Single shot record scan frequency analysis │
│ The static correction of first arrival refraction │- - - -      │ ② Single shot record spectrum analysis │
└─────────────────────────────────────┘             └─────────────────────────────────────┘
                          │
                          ▼
┌─────────────────────────────┐
│ Regional anomaly processing │
└─────────────────────────────┘
                          │
                          ▼
┌─────────────────────────────────┐
│ Spherical spreading compensation │
└─────────────────────────────────┘
                          │
                          ▼
┌───────────────────────────────────────┐
│ Surface consistent amplitude compensation │
└───────────────────────────────────────┘
                          │
                          ▼
┌──────────────────────────────────────────────────────────┐      ┌─────────────────────────────────┐
│ Remove the low speed inclined interference by the method of *f-k* │- - ->│ ③ Single shot record spectrum analysis │
└──────────────────────────────────────────────────────────┘      └─────────────────────────────────┘
                          │
                          ▼
┌──────────────────────────────┐
│ Surface consistent deconvolution │
└──────────────────────────────┘
                          │
                          ▼
┌─────────────────────────┐                                        ┌─────────────────────────────────┐
│ Zero phase deconvolution │- - - - - - - - - - - - - - - - - - - ->│ ④ Single shot record spectrum analysis │
└─────────────────────────┘                                        └─────────────────────────────────┘
                          │
                          ▼
┌────────────────────────────────────────┐
│ Velocity analysis and space-variant resection │
└────────────────────────────────────────┘
                          │
                          ▼
┌─────────────────────────┐
│ Residual static correction │
└─────────────────────────┘
                          │
                          ▼
┌───────────────┐
│ Superposition │
└───────────────┘
                          │
                          ▼
┌─────────────────────────┐     ┌────────┐
│ Zero phase deconvolution │────>│ Offset │
└─────────────────────────┘     └────────┘
                          │           │
                          ▼           ▼
┌─────────────────────────┐     ┌─────────────────────────┐
│ Random noise attenuation │     │ Random noise attenuation │
└─────────────────────────┘     └─────────────────────────┘
                          │           │
                          ▼           ▼
┌───────────────────────────┐   ┌───────────────────────┐       ┌─────────────────────────┐
│ Superposition results display │ │ Migration results display │- - - ->│ ⑤ Migration results display │
└───────────────────────────┘   └───────────────────────┘       └─────────────────────────┘
```

Figure 1.3 Seismic data high resolution and high SNR processing.

noise elimination, we used the single shot record and the spectrum analysis results of target layer (control point ③, Figure 1.6) to analyze the effect of noise elimination. After finishing zero phase deconvolution process, we used the single shot record and the analysis results on spectrum of target layer (control point ④, Figure 1.7) to analyze the effect of zero phase deconvolution; after completing the migration process, we used the stacked migration profile and the spectrum analysis results of target layer (control point ⑤, Figure 1.8) to analyze the effect of increasing the resolution.

In Figure 1.4, the original single shot record frequency scan (control point ① in Figure 1.3) is used to analyze the quality of original seismic data, and to analyze the single shot record of $0 \sim 20\,Hz$ scanning at the same shot point from different seismic source.

A little signal (or noise) can be observed in the single shot record of $5 \sim 8\,Hz$ scanning under single deep well excitation and in the single shot record of $3 \sim 6\,Hz$ scanning under combined well excitation, while no signal (or noise) can be observed in the single shot record below $8\,Hz$ scanning under controllable seismic source excitation, indicating the loss of low-frequency component (the scanning frequency of controllable seismic source excitation is $8 \sim 90\,Hz$).

Figure 1.4b shows the analysis on single shot records of $10 \sim 120\,Hz$ scanning at the same shot point of different seismic sources. Signals can be observed in the single shot record of $5 \sim 100\,Hz$ scanning of single deep well excitation. Signals can be observed in the single shot record of $4 \sim 80\,Hz$ scanning under combined
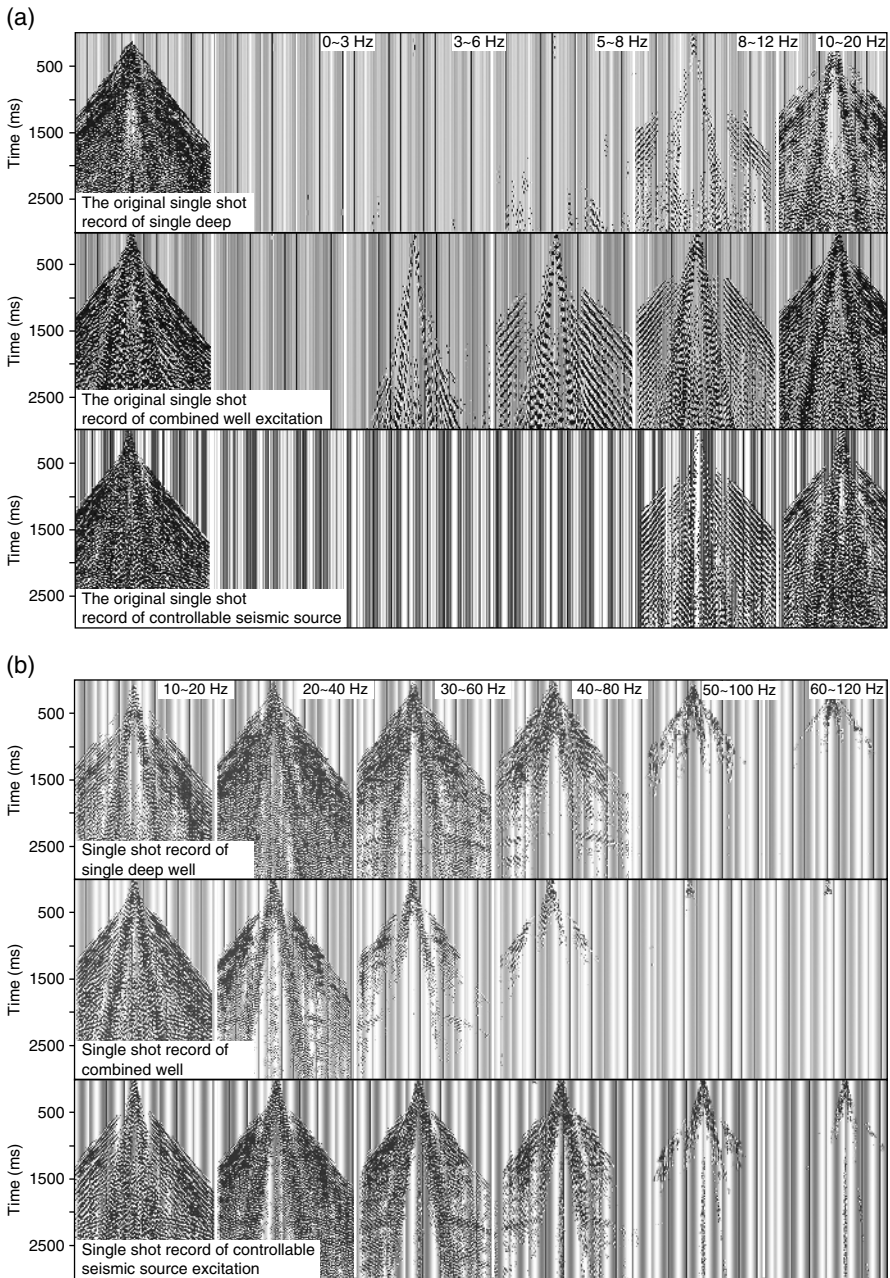
(a)

(b)

Figure 1.4 Single shot records at same shot point of different seismic sources. (a) Analysis on 0~20 Hz scanning. (b) Analysis on 10~120 Hz scanning.

well excitation. Signals can still be observed in the single shot record of 8~100 Hz scanning under controllable seismic source excitation.

From the perspective of scanning signal, single deep well and controllable seismic source excitation have wide frequency bandwidth, while combined well
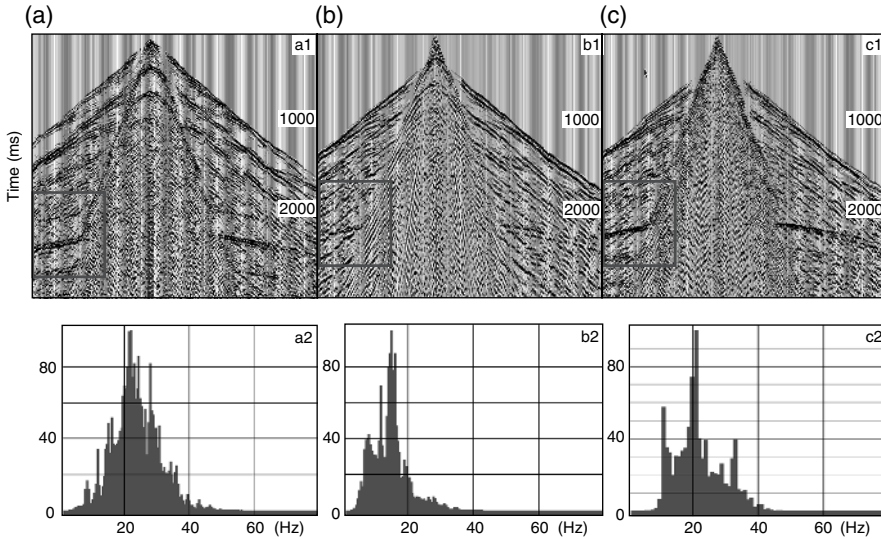
Figure 1.5 Analysis results on single shot record and frequency spectrum of target layer processed by static correction of first arrival refraction.

excitation has narrow bandwidth; low frequency component below 8 Hz is missing in controllable seismic source excitation.

Figure 1.5 shows the analysis results on the single shot record (control point ② in Figure 1.3, selects the same point for excitation and compares the original single shot records excited by different seismic sources) and seismic spectrum of target layer processed by static correction of first arrival refraction ((a) is single deep well excitation; (b) is combined well excitation; (c) is controllable seismic source excitation). From this we can see that the frequency bandwidth of single shot record under single well excitation is 4~50 Hz, with the dominant frequency at 22 Hz (Figure 1.5a); the frequency bandwidth of single shot record under combined well excitation is 4~40 Hz, with the dominant frequency at 18 Hz (Figure 1.5b); the frequency bandwidth of single shot record under controllable seismic source excitation is 8~45 Hz, with the dominant frequency at 20 Hz (Figure 1.5c).

Figure 1.6 shows the analysis results on single shot record (control point ③ in Figure 1.3, which eliminates low frequency surface wave mainly by f-k; the high frequency component is enhanced for the high intensity of eliminating low frequency components) and frequency spectrum of target layer processed by prestack noise elimination ((a) is single deep well excitation; (b) is combined well excitation; (c) is controllable seismic source excitation). From this we can see that the frequency bandwidth of single shot record under single well excitation is 10~50 Hz, with the dominant frequency at 30 Hz; the frequency bandwidth of single shot record under combined well excitation is 8~46 Hz, with the dominant frequency at 26 Hz; the frequency bandwidth of single shot record under controllable seismic source excitation is 8~50 Hz, with the dominant frequency at 30 Hz (Figure 1.6c).

Figure 1.7 shows the analysis on the single shot record and frequency spectrum of target layer at the same point from different seismic resources, which is
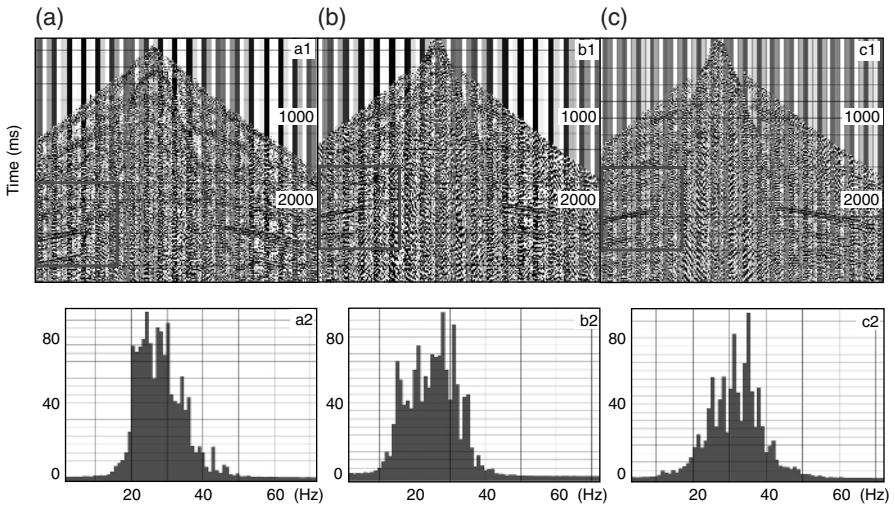
Figure 1.6 Analysis result on single shot record and frequency spectrum of target layer processed by prestack noise elimination.
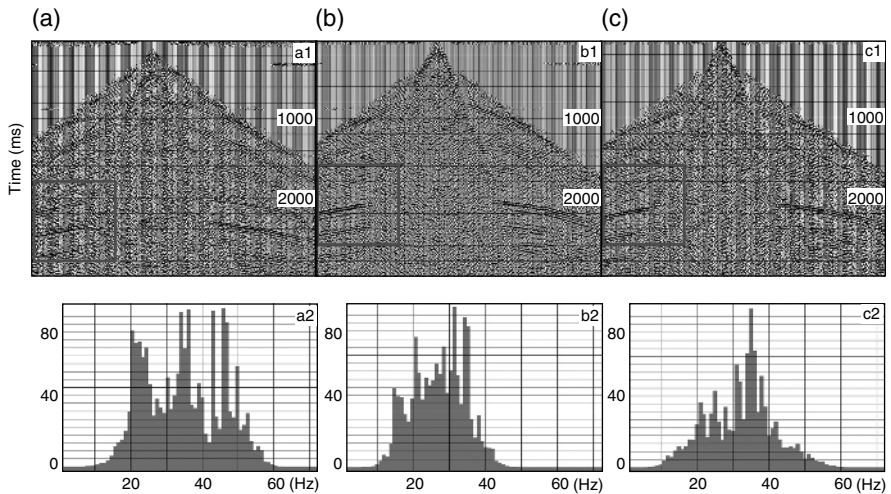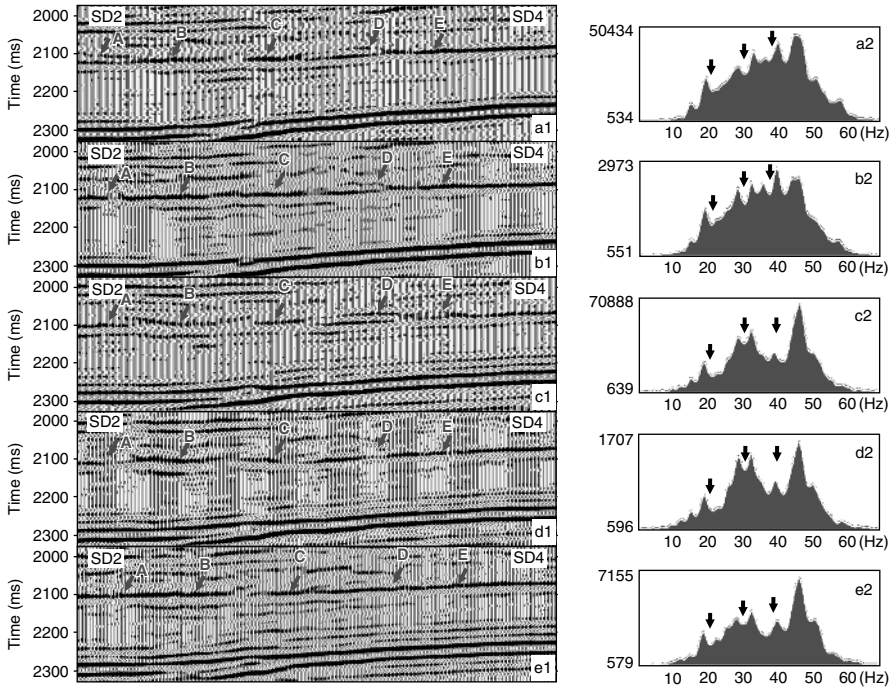

Figure 1.7 Analysis results on single shot record and frequency spectrum of target layer processed by prestack zero phase deconvolution.

obtained after zero-phase deconvolution (control point ④ in Figure 1.3) applied in the process stated in Figure 1.3 ((a) is single deep well excitation; (b) is combined well excitation; (c) is controllable seismic source excitation). From this we can see that the frequency bandwidth of single shot record under single well excitation is $10 \sim 62$ Hz, with the dominant frequency at 33 Hz; the frequency bandwidth of single shot record under combined well excitation is $8 \sim 46$ Hz, with the dominant frequency at 28 Hz; the frequency bandwidth of single shot record under combined well excitation is $8 \sim 60$ Hz, with the dominant frequency at 34 Hz.

Figure 1.8 Seismic profile and frequency spectrum of target layers processed by high resolution and high SNR processing.

The zero phase deconvolution widens frequency bandwidth of target layer seismic record and improves the dominant frequency. It is obvious that the single deep well excitation and controllable seismic source excitation have wide frequency bandwidth and high dominant frequency, compared to these of combined well excitation.

From the analysis results on the frequency bandwidth and the dominant frequency of target layer recorded in single shot records in Figures from 1.4 to 1.7, the frequency bandwidth of single deep well excitation and controllable seismic source excitation are wide (low frequency component below 8 Hz is missed in controllable seismic source excitation) and the dominant frequencies are high, while those of combined well excitation are narrow and low. Therefore, the performance of single deep well excitation and controllable seismic source excitation are better than that of combined well excitation.

Figure 1.8 shows a final image in the form of migration profile based on the procedures presented in Figure 1.3 (control point ⑤ in Figure 1.3 uses poststack deconvolution parameters to widen the frequency bandwidth to the uniform bandwidth).

Figure 1.8a1 is a final migration profile of single deep well excitation (channel interval of 5 m) obtained from processes indicated in Figure 1.3. In Figure 1.8a1, the reflection event marked by red arrows refers to the reservoir of the Cretaceous Qingshuihe river sand formation. This image clearly presents the geological phenomenon of lateral sand body variation. Figure 1.8a2 is a frequency spectrum of the target layer(2050 ~ 2150 ms), with a frequency bandwidth of 8 ~ 65 Hz and a dominant frequency of 40 Hz.

Figure 1.8b1 shows one final migration profile of a single deep well excitation (channel interval of 5 m) obtained from processes presented in Figure 1.3. Obviously, the lateral resolution of the Cretaceous Qingshuihe river sand formation reflection marked by red arrows in this figure is lower than that of Figure 1.8a1. Although different from the resolution, the spectrums (Figure 1.8a2, Figure 1.8b2) of the target layers (2050~2150 ms) are almost the same, which suggests that the longitudinal resolutions are the same. The lateral resolution directly depends on the channel interval of the research samples; therefore, it is clear that the lateral resolution of a 5 m channel interval is higher than that of a 25 m interval.

Figure 1.8c1 shows the final migration profile of combined well excitation (channel interval of 5 m) obtained from processes presented in Figure 1.3. The Cretaceous Qingshuihe river sand formation reflection marked by red arrows in this figure is similar to that in Figure 1.8a1, while its energy is relatively weak and its lateral resolution is relatively high. Figure 1.8c2 is a frequency spectrum of the target layer (2050~2150 ms), with a frequency bandwidth of 8~65 Hz and a dominant frequency of 35 Hz.

Figure 1.8d1 shows a final migration profile of combined well excitation (channel interval of 25 m) obtained from processes presented in Figure 1.3. It is obvious that its lateral resolution is lower than that of Figure 1.8c1. The fact that the frequency characteristics presented in Figure 1.8c2 and Figure 1.8d2 are almost the same suggests that the lateral resolution directly depends on the channel interval of the research samples if the longitudinal resolutions are the same. Accordingly, the lateral resolution of a 5 m channel interval is higher than that of a 25 m interval. On comparison between Figure 1.8c2 (Figure 1.8d2) and Figure 1.8a2 (Figure 1.8b2), we can see segments of low frequency (marked by blue arrows) in the range of 35 Hz and 42 Hz. This difference shows that the frequency components of combined well excitation are less abundant than that of single deep well excitation.

Figure 1.8e1 shows a final migration profile of controllable seismic source excitation (channel interval of 25 m) obtained from processes presented in Figure 1.3. Obviously, the Cretaceous Qingshuihe river sand formation reflection marked by red arrows in this figure can be regarded as a strong one, which is much worse in description of sand body details compared with Figures 1.8a1 to 1.8d1.

Figure 1.8e2 is a frequency spectrum of the target layer (2050~2150 ms), with a frequency bandwidth of 8~65 Hz and a dominant frequency of 35 Hz. Compared with Figures 1.8a2 (Figure 1.8b2), it has two segments of low frequency (marked by blue arrows) and a lack of frequency components blow 8Hz.

The frequency bandwidth of controllable seismic source excitation is wider than that of combined well excitation (Figure 1.4 and Figure 1.5), but its frequency components are less abundant. Additionally, low frequency components below 8 Hz are missing, resulting in a single waveform of migration result, with which it is difficult to accurately reflect the spatial distribution characteristics of lithology.

The processes in Figure 1.3 focus too much on high resolution and high SNR processing. Therefore, both prestack and poststack deconvolutions have been applied. In order to ensure the continuity of high-resolution profiles processed

by deconvolution, random noise attenuation (RNA) has also been employed, which gives out a good visual effect of migration profiles but greatly decreases the fidelity. We will have to make further analysis to see whether the real seismic response of the Cretaceous Qingshuihe river sand formation is as shown in Figure 1.8.

1.3   Discussion on the Cause of Notching

The scale of seismic data resolution is restricted by the signal to noise ratio of seismic signals. During the resolution enhancement processing of seismic data, if the signal to noise ratio of seismic signals is small (SNR is less than 1), the credibility of processed high-resolution data is very low.

Among the effective frequency band of seismic record, the SNR of seismic signals is usually larger than 1; the SNR of high frequency components which are beyond such effective frequency band is generally less than 1. Where the data in high-frequency band (SNR is less than 1), the deconvolution method is adopted to boost its energy. As a consequence, it amplifies noise energy significantly while boosting the effective signals. When promoted SNR random noise attenuation modification (RNA) is applied to such seismic data with amplified high frequency noise, such high frequency noises are easy to change into some lateral extended high frequency events. But this is only a false image and can mislead the interpretation.

Figure 1.9 shows the results comparison of random noise data processed two times with RNA method repeatedly.
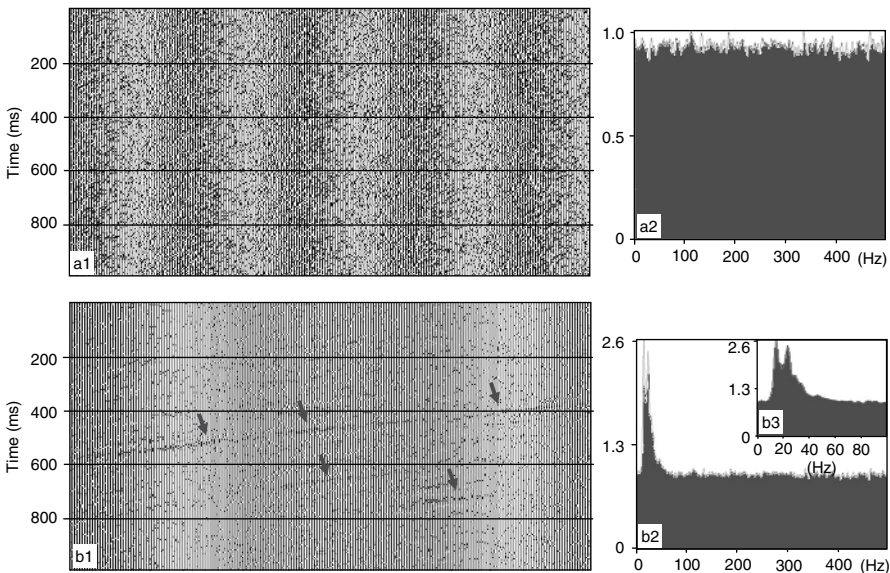
Figure 1.9 Results comparison of random noise data processed two times with RNA method repeatedly.

Figure 1.9a1 shows the random noise profile with record length of 1 s (sampling at 1 ms) and channel interval of 25 m.

Figure 1.9a2 shows the spectrum of Figure 1.9a1, with a range of $0 \sim 500$ Hz and a spectral value of almost 0.9, which belongs to typical white noise spectrum.

Figure 1.9b1 shows the processing results of the random noise data of Figure 1.9a1 after two successive RNA (i.e. coherence enhancement, such a modifying module, is commonly used to boost S/N, and such a module is also adopted in the processing flow of Figure 1.3), and some laminar reflections are clearly discerned on the profile (as indicated by a red arrow).

Figure 1.9b2 is the spectrum of Figure 1.9b1, and Figure 1.9b3 is the local zoom of Figure 1.9b2, which highlights the spectrum features of $0 \sim 100$ Hz. The spectrum features of $10 \sim 40$ Hz share the same frequency band with the effective seismic signals, and its energy is nearly three times that of white noise spectrum. Such laminar reflection caused by modification processing is only a false image, and it impacts seismic interpretation directly. Such a false image can be interpreted as a thin layer in seismic interpretation, and its spectrum is hard to distinguish in the effective frequency band range. Therefore, it is suggested that such a module is excluded in relative fidelity preservation processing, as the resulting profile visual effect is relatively poor.

During the frequency spectrum analysis of seismic data processing, notch frequency is frequently observed in seismic record spectrum, which may be caused by the frequency response of the geological body itself (a section of frequency is absent). Such phenomenon is quite normal in an effective frequency band (the seismic record in an effective frequency band has a relatively high SNR, and it can be used to analyze whether the notch frequency is the response of the geological body). There is another kind of notch frequency existing on the high frequency band portion, which is no lower than the effective frequency band. It may be caused by the high-pass filtering of the deconvolution operator, which was the object of this study.

The processing flow in Figure 1.3 overemphasizes high resolution and high SNR; therefore, two episodes of deconvolution (prestack and poststack) have been conducted. In order to ensure the profile continuity after high resolution deconvolution, RNA has been performed to realize a better visual effect. However, the fidelity obviously reduces, such as the seismic response distortion of sand body (Figure 1.1a) and thin layer at point D of Figures 1.8a1 and 1.8c1, which deserve to be studied further.

1) The approximate expression of prestack and poststack deconvolution filters. To analyze whether the notch frequency phenomena (as indicated by blue arrows in Figures 1.8c2, b2 and e2) in the frequency spectrum of target layer ($2000 \sim 2200$ ms) in the final migration profile is the frequency response of the geological body itself, or the consequence of the deconvolution operator high-pass filtering (as shown in the processing flowchart of Figure 1.3, prestack zero-phase deconvolution is conducted to increase the resolution after surface consistent deconvolution; and after stack, another zero phase deconvolution is conducted to further increase the resolution), the prestack and poststack zero phase deconvolutions should be analyzed.

If the seismic record is assumed to be:

$$S(t) = r(t) * g(t) \tag{1.1}$$

Where, $S(t)$ is the seismic signal; $r(t)$ is the reflection factor; $g(t)$ is the seismic wavelet.

Equation 1.1 is written in frequency domain as:

$$S(\omega) = r(\omega) * g(\omega) \tag{1.2}$$

If prestack deconvolution operator is expressed as $F_1(\omega)$ in frequency domain, the seismic signal after prestack deconvolution will be:

$$f_1(\omega) = F_1(\omega) \cdot S(\omega) = r(\omega) \cdot F_1(\omega) \cdot g(\omega) \tag{1.3}$$

Deconvolution is used to compress $g(\omega)$, so that the seismic signal is close to reflection factor to bring a higher resolution. From equation 1.3, we get:

$$F_1(\omega) = f_1(\omega) / S(\omega) \tag{1.4}$$

According to the processing flow in Figure 1.3, after prestack noise elimination in *f-k* and surface consistent deconvolution, another zero-phase deconvolution is also conducted to increase the resolution, and $F_1(\omega)$ in equation 1.4 is the embodiment of such composite filtering effect. However, the main contribution of high frequency filtering is zero phase deconvolution filter. Thus, to facilitate the discussion, $F_1(\omega)$ is almost equivalent to the prestack zero phase deconvolution filter.

Poststack deconvolution is conducted on the basis of prestack deconvolution. The operator of post-pack deconvolution is $F_2(\omega)$, and the signal spectrum after deconvolution is:

$$f_2(\omega) = F_2(\omega) \cdot f_1(\omega) = r(\omega) F_2(\omega) \cdot F_1(\omega) \cdot g(\omega) \tag{1.5}$$

From equation 1.5, we get:

$$F_2(\omega) = f_2(\omega) / f_1(\omega) \tag{1.6}$$

According to the processing flowchart in Figure 1.3, the velocity analysis, space variant removal, residual static correction, stack and migration are conducted after prepack deconvolution is completed. Finally, another zero phase deconvolution is conducted to increase the resolution, and $F_2(\omega)$ in equation 1.6 is the embodiment of such composite filtering effect. However, the main contribution of high frequency filtering is also a zero phase deconvolution filter. Thus, to facilitate the discussion, $F_2(\omega)$ is almost equivalent to the prestack zero phase deconvolution filter.

2) Description on notch frequency band.

If the maximum frequency value of the low frequency end of notch frequency band (as indicated by green arrow in Figure 1.10) is XF_{Lmax}, with the minimum frequency value at XF_{min}, the average frequency of low frequency end will be:

$$XF_L = \frac{XF_{L\max} + XF_{\min}}{2} \tag{1.7}$$

If the maximum frequency value of the high frequency end of notch frequency band is $XF_{H\max}$, with the minimum frequency value at $XF_{\min}$, the average frequency of high frequency end will be:

$$XF_H = \frac{XF_{H\max} + XF_{\min}}{2} \tag{1.8}$$

3) The width of notch frequency band is defined as:

$$XF = XF_H - XF_L \tag{1.9}$$

If the maximum frequency value of the low frequency end of notch frequency band (as indicated by green arrow in Figure 1.10) is $XF_{L\max}$, with the maximum frequency value of its high frequency end at $F_{H\max}$, the notch frequency band minimum value between the maximum values of low frequency and high frequency is $F_{\min}$.

4) The relative amplitude of notch frequency band is defined as:

$$P_F = \frac{2F_{\min}}{XF_{L\max} + XF_{H\max}} \tag{1.10}$$

Figure 1.10 shows the location of the notch frequency band in the seismic frequency spectrum. The blue dashed line illustrates the maximum value of the ultimate seismic frequency spectrum of the high frequency end (DF_H) of original seismic spectrum effective band width (DF), with its left side notch frequency band within the effective bandwidth, and its right side as the extension of such
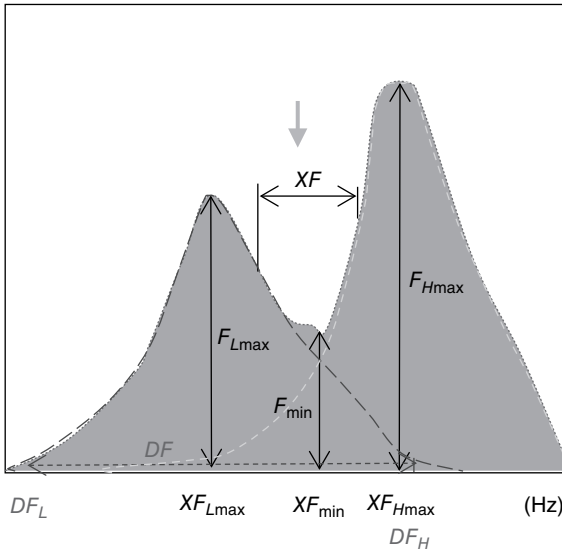
Figure 1.10 The location of notch frequency band in seismic frequency spectrum.

frequency band. The deconvolution method (green dashed line, the spectrum of the deconvolution operator) is adopted to increase the frequency band energy, especially for this type of high frequency band data (SNR is less than 1). As a consequence, the effective signals are enhanced, while the noise energy is amplified significantly. The lower the SNR, the higher noise energy is obtained, which hinders the processing of high-resolution seismic data. Therefore, the relative fidelity preservation processing should be analyzed and determined based on the notch frequency phenomena of high frequency band to ensure the reliability of seismic data processing.

Figure 1.11 is the effect comparison between a prestack and poststack deconvolution filter in a single deep well during the study on high resolution and high SNR processing within frequency domain.

Figure 1.11a shows the frequency spectrum of a single deep well (for frequency spectrum in Figure 1.5a2, smoothing processing is applied to facilitate calculation), with frequency bandwidth of $4 \sim 50$ Hz and dominant frequency of 22 Hz.

Figure 1.11b is the prestack deconvolution filtering operator $F_1(\omega)$, with frequency bandwidth of $30 \sim 60$ Hz and dominant frequency of 48 Hz, which is a typical high frequency band-pass filter. Compared with $F_1(\omega)$ spectrum, the red dotted line in Figure 1.11a shows different dominant frequency (22 Hz, 48 Hz), and the frequency difference is 26 Hz. There is an obvious non-overlapped area (as indicated by green arrow) in $30 \sim 45$ Hz between the dominant frequencies; in $0 \sim 30$ Hz, the low frequency value of operator is very small (as indicated by green arrow), which suppresses the low frequency information.
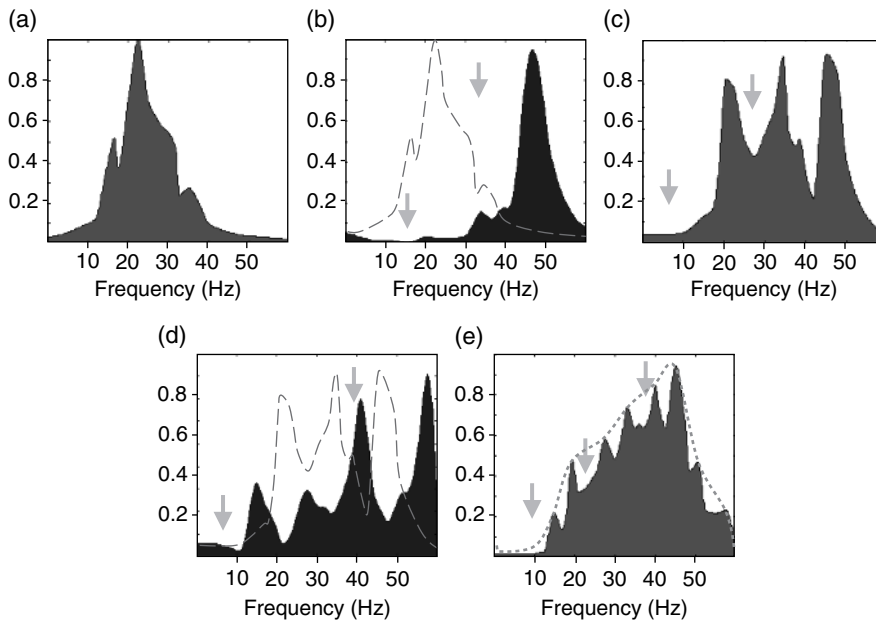

Figure 1.11 Filter frequency spectrum comparison between pre-pack and post-pack deconvolutions in single deep well.

Figure 1.11c shows the frequency spectrum after prepack deconvolution (for frequency spectrum in Figure 1.7a2, smoothing processing is applied to facilitate calculation), where there is a notch frequency in $0 \sim 12\,\text{Hz}$, a weak notch frequency in $20 \sim 30\,\text{Hz}$ with XF of $5\,\text{Hz}$ and P_F of 31% and a severe notch frequency at $40\,\text{Hz}$ with XF of $10\,\text{Hz}$ and P_F of 74%.

Figure 1.11d is postpack deconvolution operator $F_2(\omega)$, which is a wide band filter, with frequency bandwidth of $10 \sim 60\,\text{Hz}$ and dominant frequency of $40\,\text{Hz}$. Its spectrum is nearly identical to that of the red dashed line in frequency band of $10 \sim 50\,\text{Hz}$.

Figure 1.11a and Figure 1.11c show the frequency spectrum of single shot recorded target layer ($1800 \sim 2800\,\text{ms}$), and Figure 1.11e is the spectrum of migration profile target layer ($2000 \sim 2200\,\text{ms}$); there is a certain amount of error between them (the error is within 5%, which makes no impact on analysis results), and the red dotted line is the envelope line of such spectrum; no obvious notch frequency is observed on such a line, its frequency bandwidth is $10 \sim 68\,\text{Hz}$, dominant frequency is $40\,\text{Hz}$, and the widened high frequency is $18\,\text{Hz}$.

Figure 1.12 shows the effect comparison between prestack and poststack deconvolution filter in combined well during the study on high-resolution and high-SNR processing within frequency domain.

Figure 1.12a shows the frequency spectrum of combined well (for frequency spectrum in Figure 1.12a, smoothing processing is applied to facilitate calculation), with frequency bandwidth of $4 \sim 40\,\text{Hz}$ and dominant frequency of $18\,\text{Hz}$.
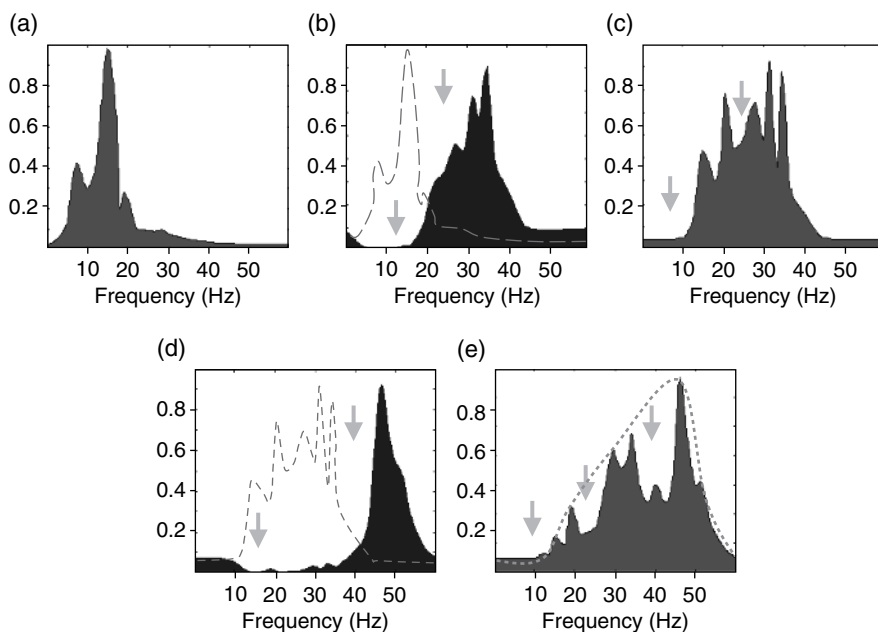

Figure 1.12 Filter frequency spectrum comparison between prepack and post-pack deconvolutions in combined well.

Figure 1.12b is the prestack deconvolution filtering operator $F_1(\omega)$, with frequency bandwidth of $18 \sim 50$ Hz and dominant frequency of 38 Hz, which is a typical high-frequency filter. Compared with $F_1(\omega)$ spectrum, the red dotted line in Figure 1.12a shows different dominant frequency (18 Hz, 38 Hz), with the frequency difference at 20 Hz. There is an obvious non-overlapped area (as indicated by green arrow) in $18 \sim 38$ Hz between the dominant frequencies; in $0 \sim 18$ Hz, the low frequency value of operator is very small (as indicated by green arrow), which suppresses the low frequency information.

Figure 1.12c shows the frequency spectrum after prepack deconvolution (for frequency spectrum in Figure 1.7b2, smoothing processing is applied to facilitate calculation), where there is a notch frequency in $0 \sim 12$ Hz and a weak notch frequency in $20 \sim 30$ Hz with XF of 5 Hz and P_F of 31%.

Figure 1.12d is the postpack deconvolution operator $F_2(\omega)$, which is a high frequency filter, with frequency bandwidth of $35 \sim 60$ Hz and dominant frequency of 47 Hz. There is an obvious non-overlapped area (as indicated by green arrow) between the spectrum of such filter and the red dashed line in $35 \sim 45$ Hz (the dominant frequency in Figure 1.12c is about 30 Hz, and the dominant frequency difference is 17 Hz). Therefore, an obvious notch frequency is formed (as indicated by green arrow at 40 Hz in Figure 1.12e). Meanwhile, the notch frequencies in $0 \sim 12$ Hz and $20 \sim 30$ Hz (as indicated by blue arrow in Figure 1.8c) still remain.

Figure 1.12e shows the final spectrum of target layer on the achieved profile. Figure 1.12a and Figure 1.12c are the spectrum of single shot recorded target layer ($1800 \sim 2800$ ms), and Figure 1.12e is the target layer spectrum of migration profile ($2000 \sim 2200$ ms). There is a certain amount of error between them (the error is within 5%, which makes no impact on analysis results), and the red dotted line is the envelope line of such spectrum. Three obvious notch frequencies are observed on such a line, where in $0 \sim 12$ Hz, two episodes of deconvolution suppress the low frequency below 10 Hz and result in severe notch frequency; in $20 \sim 30$ Hz, the weak notch frequency XF is 5 Hz and P_F is 31%; in $35 \sim 45$ Hz, due to the relatively narrow frequency band of combined well excitation record, the high frequency components are rare, which results in severe notch frequency with XF of 10 Hz and P_F of 56%. As for the frequency bandwidth of $10 \sim 64$ Hz, its dominant frequency is 36 Hz, and the widened high frequency is 24 Hz, which is 6 Hz higher than that of Figure 1.11e, resulting in severe notch frequencies, especially the false information in the thin layer (point D in Figures 1.8a1 and 1.8c1).

1.4   Discussion of Impact on Processing of Relative Fidelity Preservation Seismic Data for Seismic Acquisition and Observation Mode

In order to solve the actual seismic response problems of the Cretaceous Qingshuihe sand body (as shown in Figure 1.8), we put forward the relative fidelity preservation processing flow as illustrated in Figure 1.13. Compared with high-resolution and high-SNR processing flow (Figure 1.3), the relative fidelity
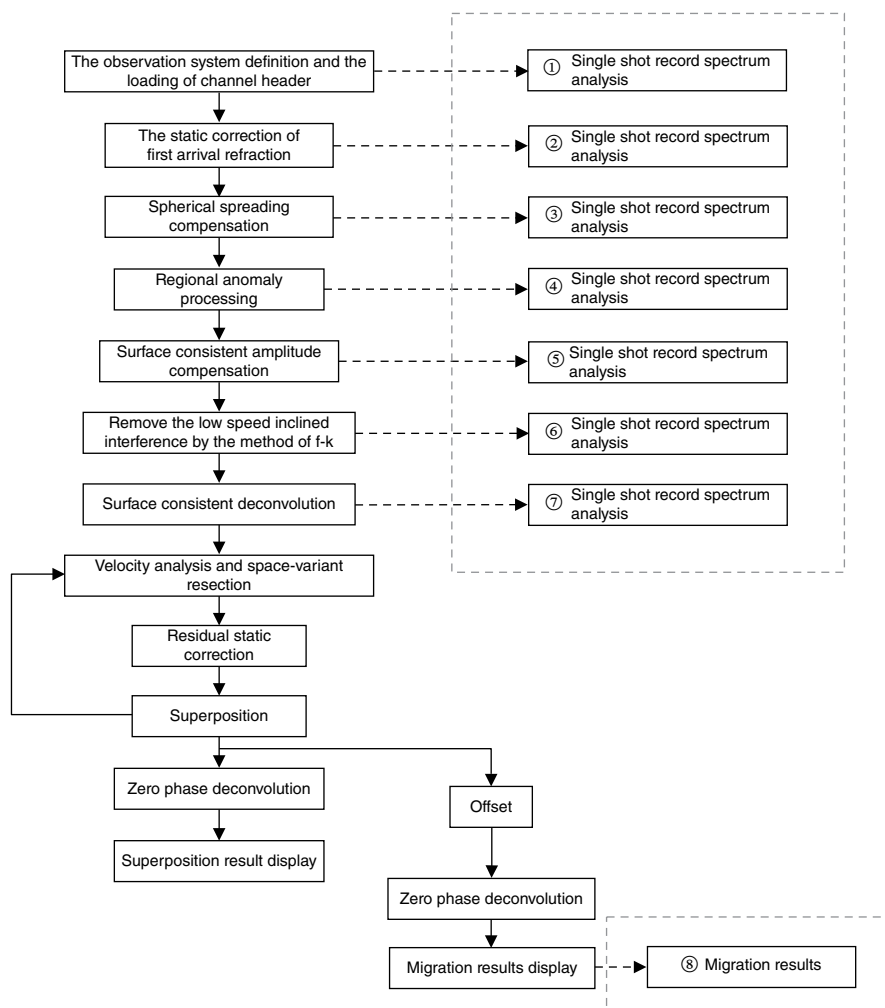
Figure 1.13 The processing flow of relative fidelity preservation seismic data.

preservation processing eliminates processes of prestack zero phase deconvolution and RNA. Additionally, 60 times of coverage are applied to facilitate the comparison.

During the relative fidelity preservation processing, eight controlling points (as shown in the dashed line box of Figure 1.13) were selected to conduct quality tracing and analysis. Relative fidelity preservation processing flow (Figure 1.13) was adopted to reprocess the seismic data of the pilot survey line across Well Shidong-2 and Well Shidong-4 in the Shidong area.

Figure 1.13 shows the single shot record of single deep well and the seismic spectrum of target layer at Well Shidong-4 (SD4), which is different from the single shot location in Figure 1.4; however, it makes no impact on analysis results. This figure also shows the single shot records and seismic spectrum of target layer at various stages as per the relative fidelity preservation processing flow in Figure 1.13.

Figure 1.14a1 shows the original single shot record ①, and the quality of original single shot is good (the spectrum is $4 \sim 50\,\text{Hz}$, and the dominant frequency is $22\,\text{Hz}$).

Figure 1.14b1 shows the single shot record ② after static correction of first arrival refraction, and the first arrival is continuous.

Figure 1.14c1 shows the single shot record ② after spherical diffusion compensation, where the entire energy compensation effect is significant.

Figure 1.14 d1 shows the single shot record ④ of regional abnormality processing, where the noise elimination effect is good.

Figure 1.14e1 shows the noise after regional abnormality processing, where no effective signal is observed in this figure.

Figure 1.14 f1 shows the single shot record ⑤ after seismic consistent amplitude compensation; compared with Figure 1.9c1, the entire energy is further compensated and the compensation effect is significant (as indicated by red arrows in Figures 1.14 f1 and 1.14 cl).

Figure 1.14g1 shows the single shot record ⑥ after f-k oblique disturbance removal, which suppresses oblique disturbance effectively.

Figure 1.14h1 shows the single shot record ⑦ after surface consistent deconvolution, where the frequency increases slightly.

Figures 1.14a2–1.14h2 show the target layer ($2000 \sim 3000\,\text{ms}$) seismic spectrum corresponding to Figures 1.14a1–1.14h1.

It is known from the spectrum that: (1) Low frequency (below $8\,\text{Hz}$) is well preserved in each step. (2) The frequency band of noise spectrum after regional abnormality processing is identical to the effective signal (Figures 1.14d2 and 1.14e2). (3) f-k oblique disturbance removal can only suppress part of the oblique disturbance energy in $15 \sim 20\,\text{Hz}$ (as indicated by blue arrow in Figure 1.14g2); the final surface consistent deconvolution promotes frequency band energy in $20 \sim 40\,\text{Hz}$ (as indicated by blue arrow in Figure 1.14h2), but fails to widen the effective seismic frequency band (the effective frequency band maintains in $4 \sim 50\,\text{Hz}$ with the dominant frequency at $22\,\text{Hz}$, and the widened frequency band is no more than $5\,\text{Hz}$), which only compensates the energy in low and high frequency bands (as indicated by blue arrow).

Figure 1.15 shows the single shot record of combined well and the seismic spectrum of target layer at Well Shidong-4 (SD4).

Figure 1.15a1 shows the original single shot record, where the quality of original single shot is good (the spectrum is $4 \sim 40\,\text{Hz}$ with the dominant frequency at $18\,\text{Hz}$).

Figure 1.15b1 shows the single shot record after first arrival refraction static correction, where the first arrival is continuous.

Figure 1.15c1 shows the single shot record after spherical diffusion compensation, where the entire energy compensation effect is significant.

Figure 1.15 d1 shows the single shot record of regional abnormality processing, where the noise elimination effect is good.

Figure 1.15e1 shows the noise after regional abnormality processing, where no effective signal is observed.

Figure 1.15f1 shows the single shot record after seismic consistent amplitude compensation; compared with Figure 1.15c1, the entire energy is further
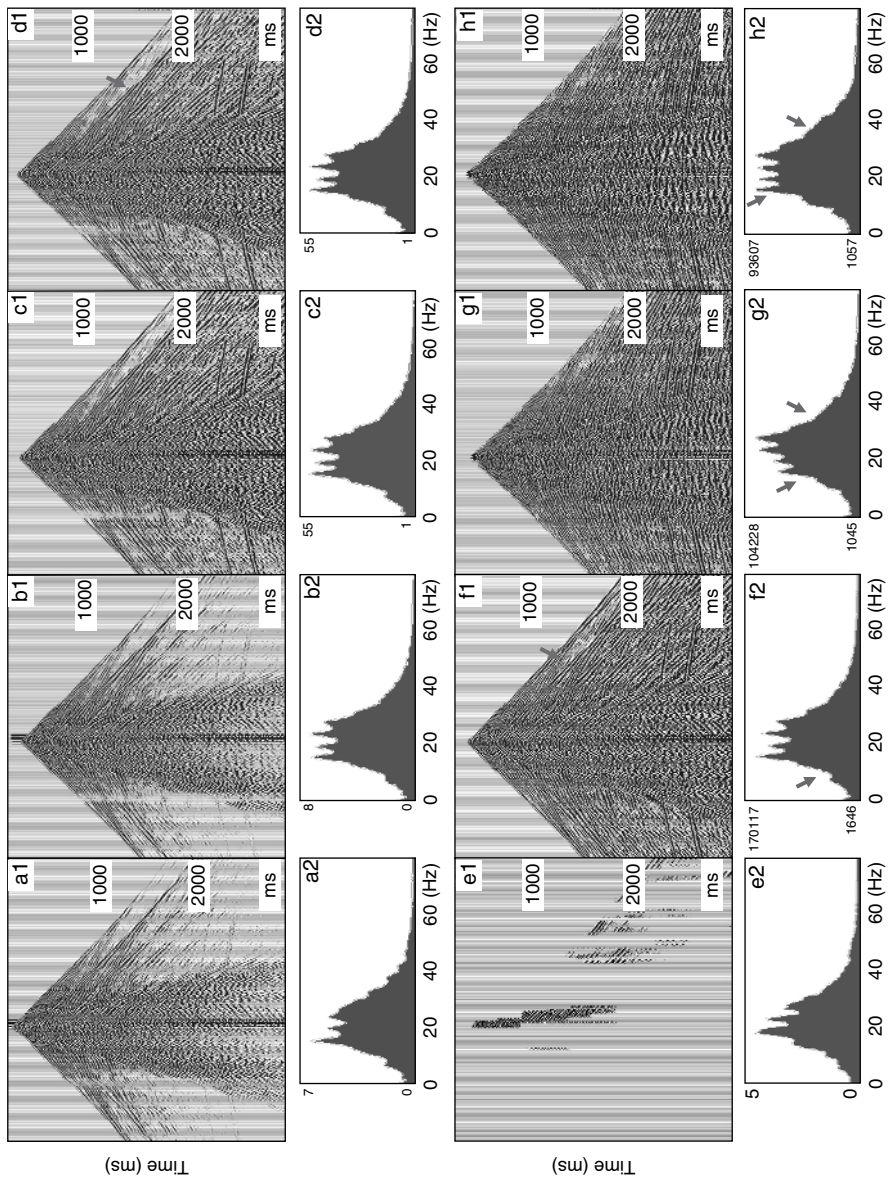
Figure 1.14 Single shot record of single deep well and seismic spectrum of target layer (SD4).
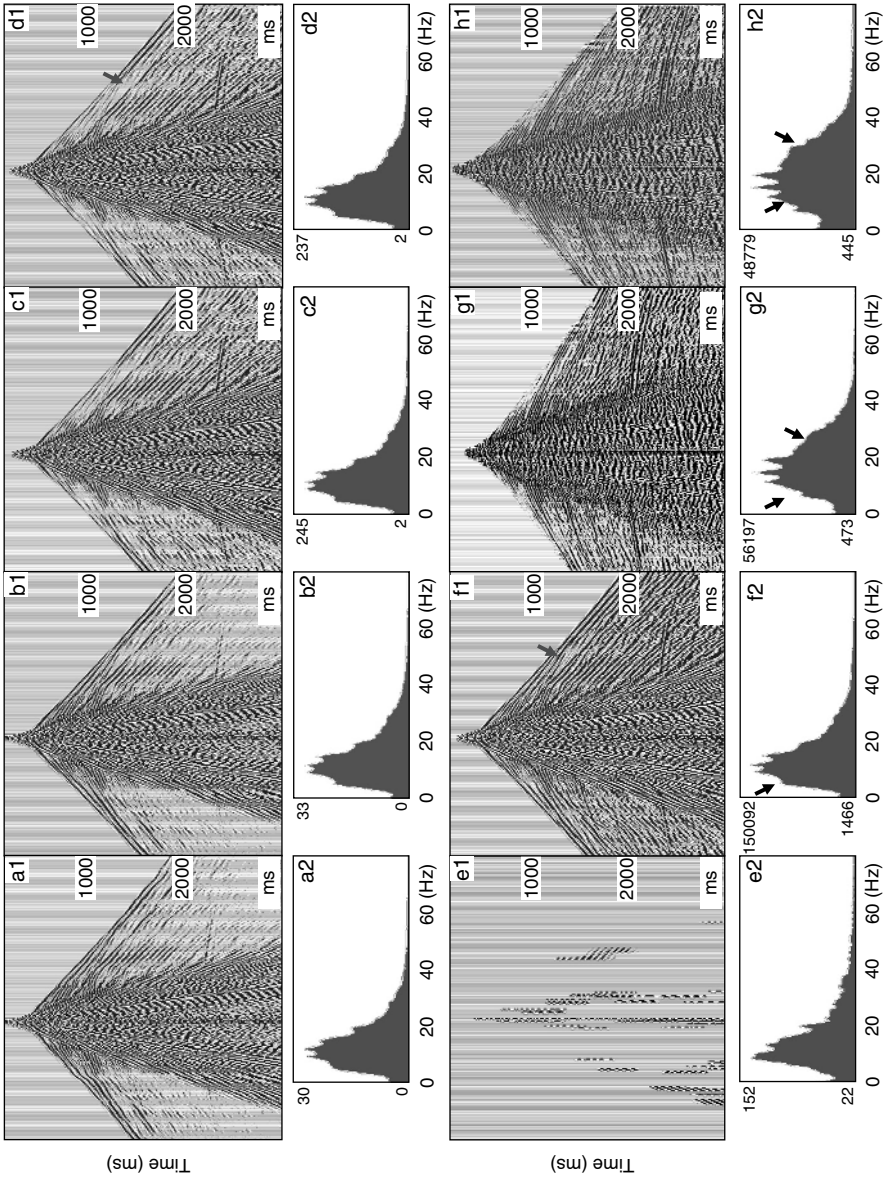
Figure 1.15 Single shot record of combined well and seismic spectrum of target layer (SD4).

compensated and the compensation effect is significant (as indicated by red arrows in Figures 1.15f1 and 1.15c1).

Figure 1.15g1 shows the single shot record after f-k oblique disturbance removal, which suppresses oblique disturbance effectively.

Figure 1.15h1 shows the single shot record after surface consistent deconvolution, where the frequency increases slightly.

Figures 1.15a2–1.15h2 show the target layer (2000~3000 ms) seismic spectrum corresponding to Figures 1.15a1–1.15h1.

It is known from the spectrum that: (1) Low frequency (below 8 Hz) is well preserved in each step. (2) The frequency band of noise spectrum after regional abnormality processing is identical to the effective signal (Figures 1.15d2 and 1.15e2). (3) f-k oblique disturbance removal can only suppress part of the oblique disturbance energy in 15~20 Hz (as indicated by blue arrow in Figure 1.15g2); the final surface consistent deconvolution promotes frequency band energy in 20~40 Hz (as indicated by blue arrow in Figure 1.15h2), but fails to widen the effective seismic frequency band (the effective frequency band maintains in 4~45 Hz with dominant frequency at 20 Hz, and the widened frequency band is no more than 5 Hz), which only compensates the energy in low and high frequency bands (as indicated by blue arrow).

Figure 1.16 shows the single shot record of controllable seismic source excitation and the seismic spectrum of target layer at Well Shidong-4 (SD4).

Figure 1.16a1 shows the original single shot record, where the quality of original single shot is good (the spectrum is 8~45 Hz with the dominant frequency is 20 Hz).

Figure 1.16b1 shows the single shot record after first arrival refraction static correction, where the first arrival is continuous.

Figure 1.16c1 shows the single shot record after spherical diffusion compensation, and the entire energy compensation effect is significant.

Figure 1.16d1 shows the single shot record of regional abnormality processing, and the noise elimination effect is good.

Figure 1.16e1 shows the noise after regional abnormality processing, and no effective signal is observed in this figure.

Figure 1.16f1 shows the single shot record after seismic consistent amplitude compensation. Compared with Figure 1.16c1, the entire energy is further compensated and the compensation effect is significant (as indicated by red arrows in figures 1.16f1 and 1.16c1).

Figure 1.16g1 shows the single shot record after f-k oblique disturbance removal, which suppresses oblique disturbance effectively.

Figure 1.16h1 shows the single shot record after surface consistent deconvolution, where the frequency increases slightly.

Figures 1.16a2–1.16h2 are the target layer (2000~3000 ms) seismic spectrum corresponding to these of Figures 1.16a1–1.16h1.

It is known from the spectrum that: (1) The low frequency components below 8 Hz are absent. (2) The frequency band of noise spectrum after regional abnormality processing is identical to the effective signal (Figures 1.16d2 and 1.16e2). (3) f-k oblique disturbance removal can only suppress part of the oblique disturbance energy in 10~20 Hz (as indicated by blue arrow in Figure 1.16g2); the final
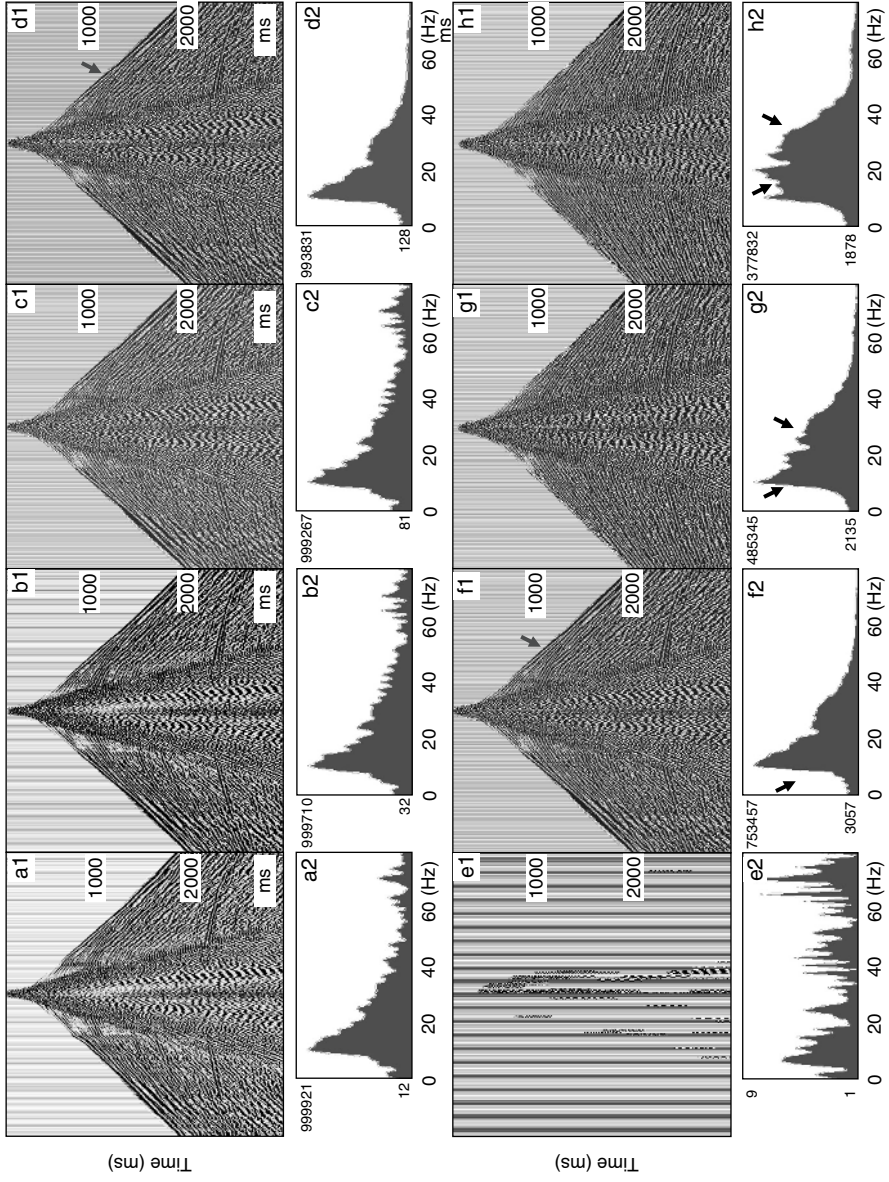
Figure 1.16 Single shot record of controllable seismic source excitation and seismic spectrum of target layer (SD4).

surface consistent deconvolution promotes frequency band energy in $20 \sim 40\,Hz$ (as indicated by blue arrow in Figure 1.16h2), but fails to widen the effective seismic frequency band (the effective frequency band maintains in $4 \sim 50\,Hz$ with the dominant frequency at $22\,Hz$, and the widened frequency band is no more than $5\,Hz$), which only compensates the energy in low and high frequency bands (as indicated by blue arrow).

Figure 1.17a1 shows the single deep well shot (receiving with 1200 channels at the channel interval of $5\,m$), which adopts the migration profile processed by relative fidelity preservation processing flow in Figure 1.13. The sand body reflection of target layer ($2000 \sim 2200\,ms$) is relatively clear (as indicated by red arrow). Its frequency bandwidth is $5 \sim 55\,Hz$ (Figure 1.17a2), and the dominant frequency is $27\,Hz$. The frequency band has not been widened, while only the dominant frequency ($27\,Hz$ or so) has been increased by $5\,Hz$.

Figure 1.17b1 shows the single deep well excitation (receiving with 240 channels at channel interval of $25\,m$), which adopts the migration profile processed by relative fidelity preservation processing flow in Figure 1.13. The sand body reflection of target layer ($2000 \sim 2200\,ms$) is relatively clear (as indicated by red arrow), while compared with Figure 1.16a1, the detailed description is slightly inferior. Its frequency bandwidth is $5 \sim 55\,Hz$ (Figure 1.16b2), and dominant frequency is $27\,Hz$, where the frequency band has not been widened, and only the dominant frequency ($27\,Hz$ or so) has been increased by $5\,Hz$.
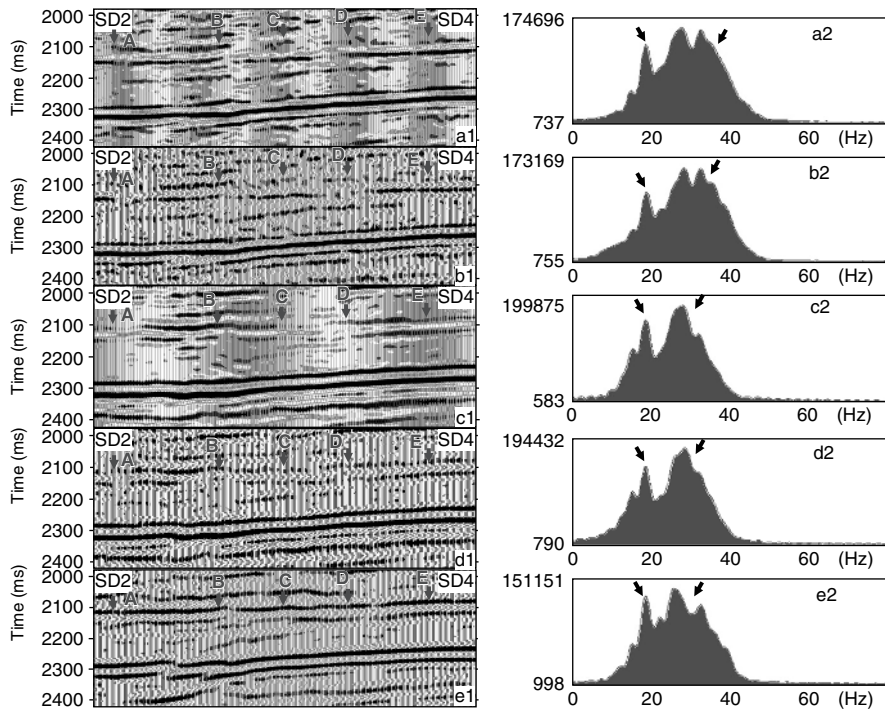

Figure 1.17 Seismic profile and target layer spectrum processed by relative fidelity preservation.

Figure 1.17c1 shows the combined well excitation (receiving with 1200 channels at channel interval of 5 m), which adopts the migration profile processed by relative fidelity preservation processing flow in Figure 1.13. The sand body reflection of target layer (2000 ~ 2200 ms) can be discerned clearly (as indicated by red arrow), and the continuity of target layer is also enhanced. Its frequency bandwidth is 4 ~ 45 Hz (Figure 1.16c2), and dominant frequency is 25 Hz, where the frequency band has not been widened, and only the dominant frequency (25 Hz or so) has been increased by 7 Hz.

Figure 1.17d1 shows the combined well excitation (receiving with 240 channels with channel interval of 25 m), which adopts the migration profile processed by relative fidelity preservation processing flow in Figure 1.13. The sand body reflection of target layer (2000 ~ 2200 ms) is relatively clear (as indicated by red arrow), and the continuity of target layer is inferior to that in Figure 1.17c1. Its frequency bandwidth is 4 ~ 45 Hz (Figure 1.16d2), and dominant frequency is 25 Hz, where the frequency band has also not been widened, and only the dominant frequency (25 Hz or so) has been increased by 7 Hz.

Figure 1.17e1 shows the controllable seismic source excitation (receiving with 300 channels at the channel interval of 25 m), which adopts the migration profile of relative fidelity preservation processing flow in Figure 1.13. The sand body reflection of target layer (2000 ~ 2200 ms) is continuous (as indicated by red arrow). Its frequency bandwidth is 8 ~ 50 Hz (Figure 1.17e2), and dominant frequency is 25 Hz. Since the controllable seismic source excitation is absent at low frequency (below 8 Hz) and high frequency (the high scan frequency is 90 Hz), the continuity of target layer is relatively strong on the seismic profile, and the detailed description is relatively poor. The frequency band has also not been widened, and only the dominant frequency (25 Hz or so) has been increased by 5 Hz.

Figure 1.18 shows the effect comparison of both single deep well prestack and poststack deconvolution filters during the study on relative fidelity preservation processing within the frequency domain.

Figure 1.18a shows the spectrum of initial stacked profile of single deep well excitation, with frequency bandwidth of 4 ~ 50 Hz and dominant frequency of about 22 Hz.

Figure 1.18b shows prestack deconvolution filtering factor $F_1(\omega)$, with frequency bandwidth of 6 ~ 60 Hz and dominant frequency of 38 Hz. It is a broad band filter (only the surface consistent deconvolution is used). In spectrum map 1.18b, there is a large overlapped area (as indicated by green arrow in Figure 1.18b) between broad band filter and red dotted line spectrum (Figure 1.18a), where the dominant frequencies are 22 Hz and 34 Hz respectively, with the frequency difference at 12 Hz. $F_1(\omega)$ filter presents some values in 0 ~ 10 Hz, which preserves the low frequency (Figure 1.18b, as indicated by green arrow).

Figure 1.18c shows the spectrum of stacked profile after prestack deconvolution, with frequency bandwidth of 4 ~ 55 Hz and dominant frequency of 25 Hz; there is no obvious notch frequency in this figure, except a weak notch frequency in 18 ~ 24 Hz with XF of 6 Hz and P_F of 37%.

In Figure 1.18d, $F_2(\omega)$ is worked out based on equation 1.6, and from the final spectrum of target layer of the achieved profile in Figure 1.18e (spectrum in
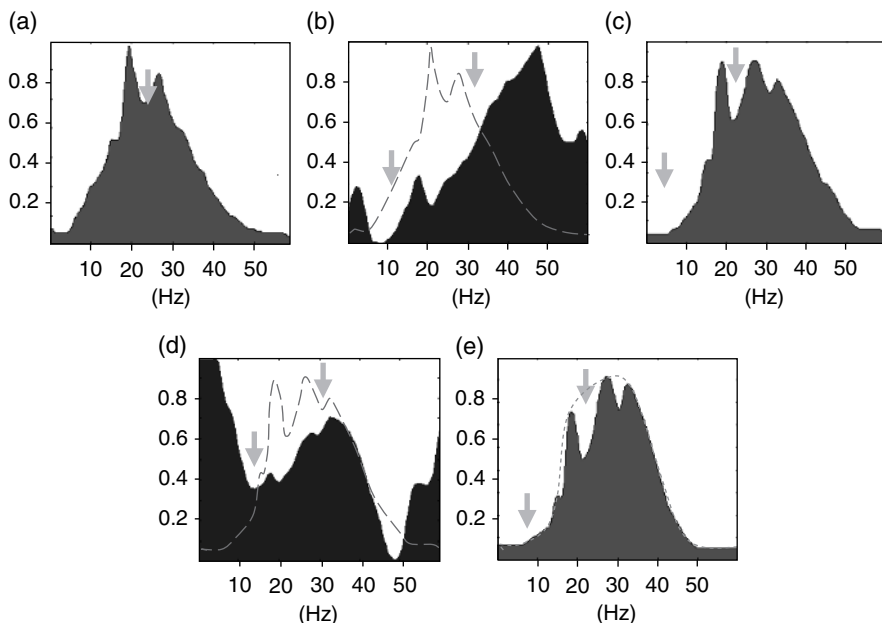
Figure 1.18 Spectrum comparison of single deep well prestack and poststack deconvolution filters.

Figure 1.17a2, smoothing processing is applied to facilitate calculation) and $f_1(\omega)$ in Figure 1.18c. Since several methods like f-k noise elimination, space variation removal and linear filtering are stacked during seismic processing, $F_2(\omega)$ is the superimposition of multiprocessing results, but it basically reflects the effect of poststack zero phase deconvolution. $F_2(\omega)$ is designed to be broad band filter, and the low frequency below 10 Hz is boosted on purpose. The filter operator nearly coincides with the red dotted line (Figure 1.18c). The processed frequency bandwidth is not widened, and only the energy of high frequency components is enhanced (Figure 1.18e).

As shown in Figure 1.18e, there is almost no notch frequency on the final spectrum of the achieved profile (Figures 1.18a, 1.18c and 1.18e show the spectrum of the target layer (2000~2200 ms) on the profile, to ensure the correctness of analysis results); the frequency band has not been obviously widened (frequency bandwidth of 4~55 Hz, widened by 5 Hz), and only the dominant frequency (about 30 Hz) has been increased by 8 Hz.

Figure 1.19 shows the effect comparison of both combined well prestack and poststack deconvolution filters during the study on relative fidelity preservation processing within frequency domain.

Figure 1.19a shows the spectrum of stacked profile of combined well excitation, with frequency bandwidth of 4~45 Hz and dominant frequency of about 18 Hz.

Figure 1.19b shows the prepack deconvolution filtering factor $F_1(\omega)$, with frequency bandwidth of 6~60 Hz and dominant frequency of 34 Hz. It is a broad band filter (only the surface consistent deconvolution is used). In spectrum map 1.19b, there is a large overlapped area (as indicated by green arrow in Figure 1.19b)
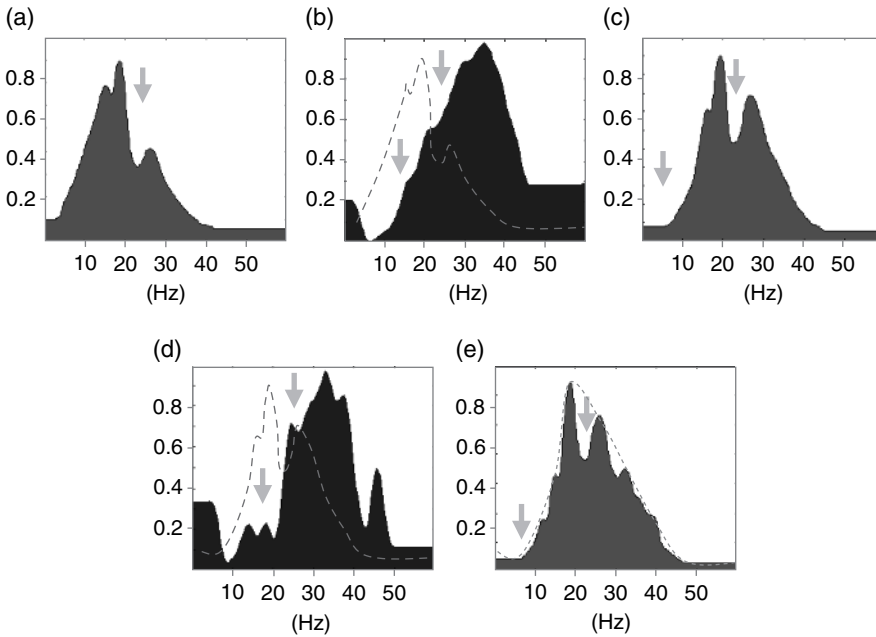
Figure 1.19 Spectrum comparison of both combined well prestack and poststack deconvolution filters.

between broad band filter and red dotted line spectrum (Figure 1.19a), whose dominant frequencies are 18 Hz and 34 Hz respectively, with the frequency difference at 16 Hz. $F_1(\omega)$ filter presents some values in $0 \sim 10$ Hz, which preserves the low frequency (Figure 1.19b, as indicated by green arrow).

Figure 1.19c shows the spectrum of stacked profile after prestack deconvolution, with frequency bandwidth of $4 \sim 45$ Hz and dominant frequency of 20 Hz; there is no obvious notch frequency in this figure, except a weak notch frequency in $18 \sim 24$ Hz with XF of 6 Hz and P_F of 37%.

In Figure 1.19d, $F_2(\omega)$ is worked out based on equation 1.6, and from the final spectrum of target layer of the achieved profile in Figure 1.17c (for spectrum in Figure 1.17c, smoothing processing is applied to facilitate calculation) and $f_1(\omega)$ in Figure 1.19c. Since several methods like f-k noise elimination, space variation removal and linear filtering are stacked during seismic processing, $F_2(\omega)$ is the superimposition of multi-processing results, but it basically reflects the effect of poststack zero phase deconvolution. $F_2(\omega)$ is designed to be broad band filter, and the low frequency below 10 Hz is boosted on purpose. The filter operator nearly coincides with the red dotted line (Figure 1.19c). The processed frequency bandwidth is not widened, and only the energy of high frequency components is enhanced.

As shown in Figure 1.19e, there is almost no obvious notch frequency on the final spectrum of the achieved profile (Figures 1.19a, 1.19c and 1.19e show the spectrum of the target layer ($2000 \sim 2200$ ms) on the profile, to ensure the correctness of analysis results); the only notch frequency is in $18 \sim 26$ Hz, with XF of

6 Hz and P_F of 37%, which is a weak notch frequency resulting from the original seismic spectrum (as indicated by green arrow in Figure 1.19a); the frequency band has not been obviously widened (frequency bandwidth 4~45 Hz, widened by 5 Hz), and only the dominant frequency (25 Hz or so) has been increased by 7 Hz.

1.5 Comparison of Results of High-resolution, High SNR Processing and Relative Fidelity Preservation Processing

Figure 1.8 shows the processing effect of high-resolution and high SNR (a1–e1) and Figure 1.17 shows the processing result of relative fidelity preservation processing (a1–e1). In the two figures, al represents single deep well excitation with channel interval of 5 m; b1 represents single deep well excitation with channel interval of 25 m; c1 represents combined well excitation with channel interval of 5 m; d1 represents combined well excitation with channel interval of 25 m; el represents controllable seismic source excitation with 300 receiving channels at channel interval of 25 m.

1) The frequency bandwidth and main frequency of target layer in Figures 1.8a2 and 1.8b2 or Figures 1.17a2 and 1.17b2 (single deep well excitation) are almost the same, the same as those in Figures 1.8c2 and 1.8d2 or Figures 1.17c2 and 1.17d2 (combined well excitation). Thus, under the same frequency bandwidth and main frequency of target layer, the horizontal and vertical resolution of the target layer reflection event will be different if the interval of receiving channel is different. It is obvious that the effects of single deep well excitation and combined well excitation with channel interval of 5 m are the best, with high horizontal and vertical resolution for target layer (especially the vertical resolution). The resolution of single deep well excitation and combined well excitation with 25 m channel interval are a little bit poor.

2) In frequency band analysis on original single shot records in Figures 1.5b2 and 1.5c2, it was believed that the data of controllable seismic source excitation was better than the data of combined well excitation at first, for the high frequency component is abundant. However, the final processing result was obviously different from explosive source, either in terms of high resolution and high SNR processing profile (Figure 1.8e1) or the relative fidelity preservation processed profile (Figure 1.17e1), which shows almost continuous reflection in the target layer (only interrupted at the fault, indicated by arrows in figure) and poor description on sand body details. The above defects are attributable to the controllable seismic source excitation itself. The target sandstone's reflection wave is superimposed by harmonic from high-frequency to low frequency, while the actual scanning frequency of controllable seismic source is 8~90 Hz (Figure 1.4b, the high frequency component of controllable seismic source scanning may be noise), so the low frequency component below 8 Hz and high frequency components above 90 Hz (Figures 1.8e2 and 1.17e2) are missing. The band is narrow and the waveform reflection of target layer is stiff.

From the point of processing profile of explosive source, the information of the target layer reflection waveform feature of single deep well or combined well is more abundant than that of controllable seismic source, especially the profile with small channel interval, which has high horizontal resolution and description accuracy. It shows the importance of broadband seismic acquisition.

3) From the point of high-resolution processed profile and relative fidelity preservation processed profile, the former has obvious advantage in resolution and SNR, but its authentic response to seismic effects on subsurface sand reservoirs may not be high. That is to say, distortion of the image is inevitable if we increase its resolution and further modify the coherence to ensure a good visual effect.

Figure 1.20a1 shows a sand interpretation mode established on the basis of the reflection characteristics of target layer presented in Figure 1.8a1.

Figure 1.20b1 is a sand interpretation mode established on the basis of the reflection characteristics of target layer presented in Figure 1.8c1, in which the thin-reservoir information is more abundant than that in Figure 1.8a1 (it may be false).

Figure 1.20a2 is a sand interpretation mode established on the basis of the reflection characteristics of target layer presented in Figure 1.17a1.

Figure 1.201b2 is a sand interpretation mode established on the basis of the reflection characteristics of target layer presented in Figure 1.17c1, which is almost the same as the characteristics in Figure 1.17a1.

From comparison between high-resolution and high-SNR processing and relative fidelity preservation processing, the following points can be obtained: (1) The former fault and breakpoint marked by A and B are less clear than the latter ones. (2) The former thin reservoir marked by D (more distinct in Figure 1.8c1) does not exist in the latter, which may be a false image formed in the process of improving resolution. (3) Point E in the former image is a weaker reflection event, representing a continuous sand layer, while the latter is comprised of two to three sand bodies. (4) A section processed with high resolution and high SNR has higher longitudinal resolution and SNR, with better visual effect (particularly, the thin-reservoir information in Figure 1.8c1, which is the most abundant; it may be false). However, false image is unavoidable if we improve the resolution and intensify the coherent processing. (5) A profile
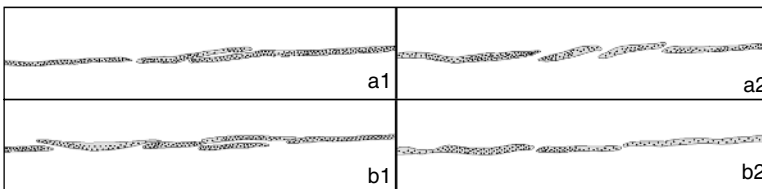

Figure 1.20 Sand interpretation based on results of high-resolution (a1, b1) and relative fidelity (a2, b2) seismic data processing. (a1,a2) single deep well, 1200 receiving channels, channel interval of 5 m; (b1,b2) combined well, 1200 receiving channels, channel interval of 5 m.

processed with relative fidelity preservation has lower longitudinal resolution and higher lateral resolution as well as lower SNR. But it can truly reflect the seismic response of subsurface sand reservoirs.

1.6   Elastic Wave Forward Modeling

Figure 1.21 shows how to analyze the reliability of profiles processed with high resolution and high SNR. Model 1 is designed as per the sand body model (to simplify the sand body model and for easy identification, Figure 1.20a1 was chosen instead of Figure 1.20b1, which contains more information on thin layers), interpreted from Figure 1.5.1a1, with the specific dimension of the model being shown by Model 1 in Figure 1.21. Model 2 is designed as per the sand body model (Figure 1.20a2 was chosen to study the lateral resolution of the sand body), interpreted from Figure 1.20a2, with the specific dimension of the model being shown by Model 2 in Figure 1.21. Refer to Figure 1.21 for the acquisition scheme, spatial location and model parameters of the elastic wave forward model. The designed elastic wave forward model focuses mainly on the research of the relation between the forward model's wavelet frequency and longitudinal resolution of the reflection event. It is necessary to show how high frequency profile is required to image the thin layer shown at point D of Figure 1.8 (a1, c1).

Provided the longitudinal resolution is $\lambda/4$ (λ is seismic wavelength), the radius of Fresnel band can be approximated to be:

$$R_0 = \lambda / 4 = v / (4 \times f) \tag{1.11}$$

Where, v is seismic velocity; f is seismic frequency.

Parameters of the model in Figure 1.17 are as follows: range of model, 12,100 m (length), 4000 m (depth); unilateral shot; wavelet frequency, 100 Hz; recording time, 3.5 s; sampling interval, 0.5 ms; number of shots, 176; shot interval, 50 m; channel interval, 10 m; length of seisline, 3000 m; maximum shot-geophone distance, 3000 m; speed for sandstone, 4100 m/s; density, 2400 kg/m^3; speed for mudstone, 3000 m/s; density, 2200 kg/m^3.

Figure 1.22 shows the prestack time migration profile (depth domain) of the elastic wave forward model (the wavelet frequency of 100 Hz and channel interval of 10 m are chosen for elastic wave forward modeling, as per equation 1.11; the lateral and vertical resolution of model parameters is about 10 m). From the profile, it can be seen that the seismic response of No. 1 sand body is clear (as shown by Model 1 in Figure 1.21); No. 1 sand body and No. 2 sand body in the figure show that the lateral resolution is higher than the lateral distance and is also higher than the channel interval (the channel interval design is also correct); the seismic trace energy between No. 1 sand body and No. 2 sand body becomes smaller; thus a sand body can be laterally identified. At the intersection between No. 2 and No. 3 sand bodies, it is impossible to identify vertically, and the reflection energy at the vertical stacked section of the two sand bodies increases, while the energy of the non-stacked section (thinner No. 2 sand body) is weak; the seismic response of No. 3 sand body is clear.
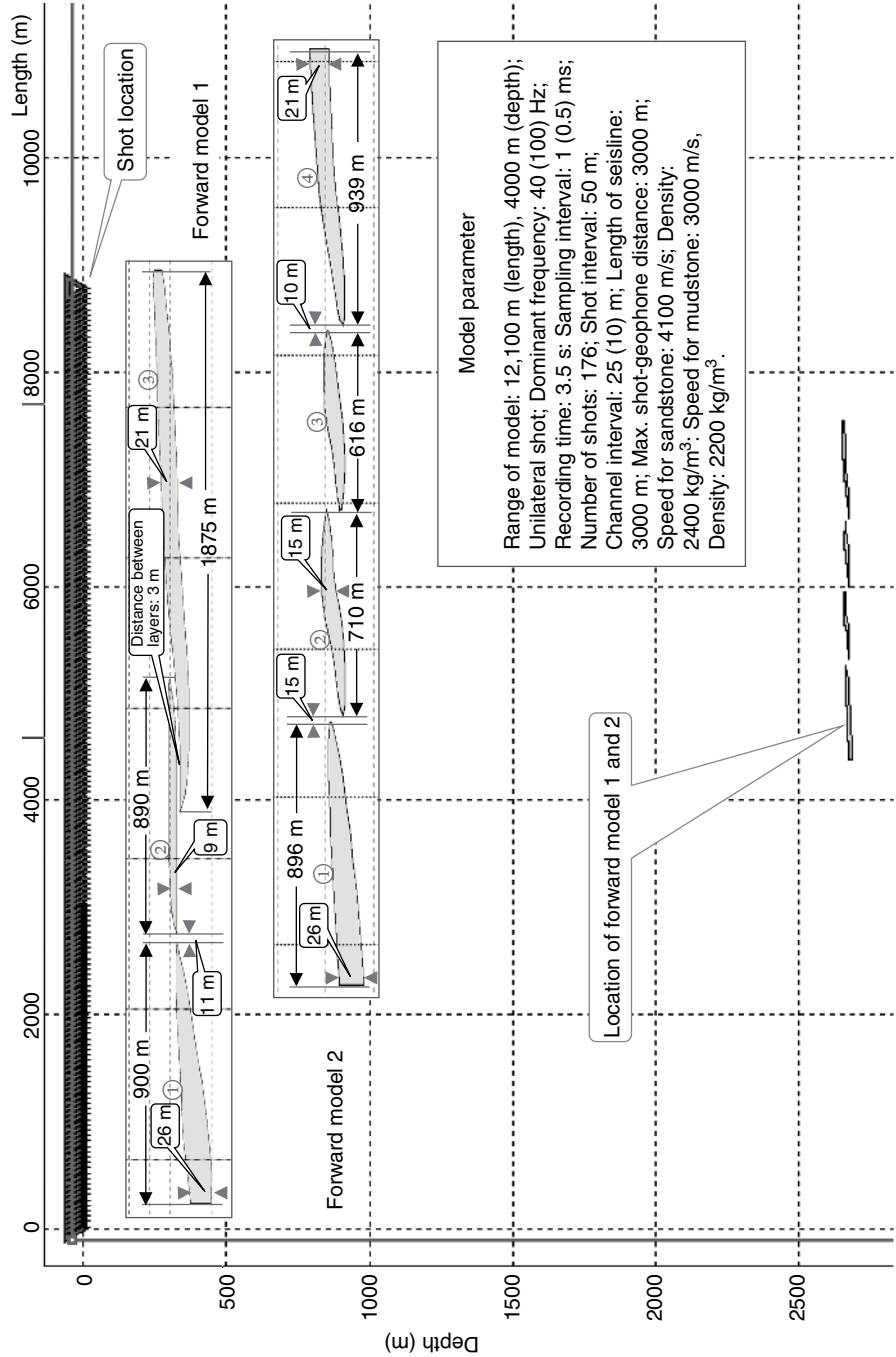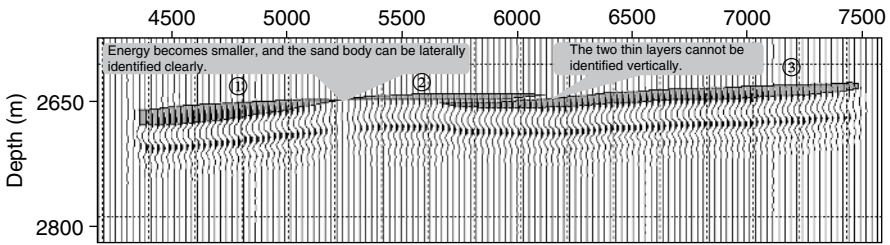
Figure 1.21 Forward model design.

Figure 1.22 Forward model 1 (100 Hz, channel interval of 10 m) prestack time migration profile (depth domain).
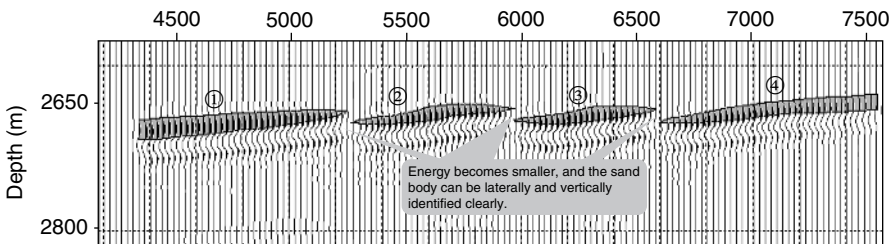

Figure 1.23 Forward model 2 (100 Hz, channel interval of 10 m) prestack time migration profile (depth domain).

The results of the elastic wave forward model suggest that the vertical resolution of the forward model with 100 Hz wavelet is unable to identify the stacked No. 2 and No. 3 sand bodies of the forward model. Actually, the frequency bandwidth and the dominant frequency of the target layer on seismic profile are only $4 \sim 55$ Hz and 25 Hz respectively (while those for the target layer of the combined well are $4 \sim 45$ Hz and 18 Hz respectively). There is something wrong with the high frequency information on the seismic profile suggested by the high resolution and high SNR results, which means that thin layers shown at point D in Figures 1.8a1 and 1.8c1 may be false.

Figure 1.23 is the prestack time migration profile of elastic wave forward model 2 (depth domain). From the profile, it can be seen that the energy at the pinch-out point of the sand body becomes low between sand body No. 1 to No. 2, No. 2 to No. 3, and No. 3 to No. 4, while the lateral distance among sand bodies (max. 15 m) is far greater than the lateral resolution (10 m), and the lateral resolution can identify the contact relationship among sand bodies.

The comparison of results from different elastic wave forward models clearly shows that the vertical resolution of the forward model with 100 Hz wavelet cannot identify the results interpreted by the seismic profile of stacked No. 2 and No. 3 sand bodies in forward Model 1. There may be some false image caused by the high resolution and high SNR processing results (thin layers shown at point D in Figures 1.8a1 and 1.8c1 may be false).

1.7 Conclusions

1) For the processed profile of explosive source, the reflection waveform feature information of target layers in either single deep well or combined well is more abundant than that of target layers in controllable seismic source profile. This is decided by the controllable seismic source itself. The reflected waves indicating target layer sandstone are formed by harmonic superimposition from high frequency to low frequency, but the actual scanning frequency of controllable seismic source is $8 \sim 90\,Hz$, lacking low frequency components below $8\,Hz$ and high frequency components above $90\,Hz$. Therefore, the frequency band is narrow and hence the reflected waveform feature on target layer is rigid, which shows the importance of seismic wideband acquisition.

2) For the profile of single deep wells or combined wells, the receiving channels are different under almost the same frequency bandwidth of target layer reflection and dominant frequency, and the longitudinal and transverse resolutions vary from each other for target layer reflected waves. It enjoys high longitudinal and transverse resolutions for target layer reflected waves received by small trace (5 m trace).

3) During exploration of lithology reservoirs, it is recommended to use the explosive source as seismic source (seismic broadband acquisition), and the small receiving channel for observation, so as to effectively identify the lithology reservoirs.

4) In view of seismic data processing for lithology reservoirs, we have come up with the relative fidelity preservation processing method, that is, four key principles for relative fidelity preservation processing of broad band: (1) Protection of effective frequency band, in principle. The widening of effective band should rely on SNR of high frequency widening components; while the high frequency widening of low SNR seismic data should be controlled (to control the bandwidth and dominant frequency of the deconvolution operator, thus preventing the noise energy at high frequency end from being amplified, will cause different level of notch frequency; deconvolution will only increase the energy of the frequency band within effective frequency band). The final spectrum of target layer of the achieved profile should not cause severe notch frequency at high frequency end (DF_H) of effective bandwidth ($XF < 6\,Hz$ and $P_F < 40\%$ as reference indexes for notch frequency control). (2) Protection of low frequency, especially that of $3–8\,Hz$. (The scenarios that suppress low frequency data of $10\,Hz$ and below in high-resolution and high-SNR processing, or significant loss of effective low frequency information with adoption of strong f-k noise elimination should be avoided.) (3) Amplitude preservation. Modification module like RNA should not be applied, to avoid damaging the lateral relationship of seismic channel amplitude. (4) Phase preservation. The module should not be used as it may damage the phase position in processing, while the zero-phase deconvolution will not damage the phase relation, and surface consistent deconvolution may adjust the phase position slightly, but will not damage the phase relation.

References

1 Wang X. The prediction and evaluation of lithological reservoir. *Geophysical Prospecting for Petroleum*, 2004, 43 (6): 511–517.

2 Wang X, Liu Q, Lv H *et al.* Application of reservoir prediction technique in the exploration and development of lithologic oil-gas reservoirs. *Petroleum Exploration and Development*, 2006, 33 (2): 189–193.

3 Wang X, Liu Q, Su M *et al.* Precision predicting reservoirs on the stages of progressive of exploration and development. *Petroleum Exploration and Development*, 2002, 29 (6): 51–53.

4 Wang X, Liu Q, Zhou J *et al.* Application of fine reservoir prediction techniques in Bannan 5-3 oilfield. *Geophysical Prospecting for Petroleum*, 2003, 42 (3): 390–394.

5 Wang X, Zhao B, Lv H *et al.* Relative amplitude preservation method for seismic data processing. *Geophysical Prospecting for Petroleum*, 2009, 48 (4): 319–331.

6 Wang X, Liu Q, Lv H *et al.* Relative amplitude method to merging processing of 3-D seismic data from multi-area. *Geophysical Prospecting for Petroleum*, 2006, 45 (2): 105–120.

7 Wang X. Research and application of statics correction modeling method in merging processing of seismic data. *Geophysical Prospecting for Petroleum*, 2006, 41 (6): 375–382.

8 Wang X, Hu Z, Tian Y *et al.* Study of seismic wavelet processing method in two-step deconvolution. *Advances in Geophysics*, 2006, 21 (4): 1167–1179.

9 Wang X. Some questions on the method of extracting high frequency information from seismic signal. *Geophysical Prospecting for Petroleum*, 2006, 41 (1): 67–75.

10 Wang X. Obtaining the high-resolution filter operator in wavelet domain. *Geophysical Prospecting for Petroleum*, 2000, 35 (3): 298–306, 314.

11 Gao J, Wang W & Zhu G. On the choice of wavelet functions for seismic data processing. *Chinese Journal of Geophysics*, 1996, 39 (3): 392–399.

12 Wang X, Gao J & Li Y. Construction of derivative wavelet function in high resolution seismic data processing. *Geophysical Prospecting for Petroleum*, 2000, 39 (2): 64–71.

13 Wang X, Liu Q, Li Y *et al.* Method of frequency division extraction of seismic signal instantaneous characteristics in wavelet domain and its application. *Geophysical Prospecting for Petroleum*, 2000, 35 (4): 452–460, 478.

14 Wang X, Liu Q, Gao J *et al.* Frequency division processing and reconstitution of seismic data in wavelet domain. *Geophysical Prospecting for Petroleum*, 2001, 36 (1): 78–85.

15 Wang X, Yang K, Zhou L, Wang J, Liu H & Li Y. Research on the computation of seismic coherence cube based on wavelet transform. *Chinese Journal of Geophysics*, 2002, 45 (6): 847–852.

16 Li Q. *The Way to Obtain a Better Resolution in Seismic Prospecting: A Systematical Analysis of High Resolution Seismic Exploration.* Beijing: Petroleum Industry Press, 1993.

17 Yu S. *High-resolution Seismic Exploration*. Beijing: Petroleum Industry Press, 1993.

18 Li Q & Zhang J. *Exploration of Lithological Oil and Gas Field—Research Method of Channel Sand Reservoir*. Qingdao: China Ocean University Press, 2006.

19 Wang X. *Wavelet Analysis Method in Seismic Data Processing and Interpretation*. Beijing: Petroleum Industry Press, 2004.